Order Number 9124164

Ultrafast optical nonlinearities in aluminum phthalocyanine organic thin films and a picosecond all-optical organic etalon switch

Williams, Valorie Sharron, Ph.D.

The University of Arizona, 1991

U·M·I
300 N. Zeeb Rd.
Ann Arbor, MI 48106

ULTRAFAST OPTICAL NONLINEARITIES IN ALUMINUM PHTHALOCYANINE ORGANIC THIN FILMS AND A PICOSECOND ALL-OPTICAL ORGANIC ETALON SWITCH

by

Valorie Sharron Williams

A Dissertation Submitted to the Faculty of the

COMMITTEE ON OPTICAL SCIENCES (GRADUATE)

In Partial Fulfillment of the Requirements
For the Degree of

DOCTOR OF PHILOSOPHY

In the Graduate College of

THE UNIVERSITY OF ARIZONA

1 9 9 1

THE UNIVERSITY OF ARIZONA
GRADUATE COLLEGE

As members of the Final Examination Committee, we certify that we have read the dissertation prepared by Valorie Sharron Williams

entitled Ultrafast Optical Nonlinearities in Aluminum Phthalocyanine Organic Thin Films and a Picosecond All-Optical Organic Etalon Switch

and recommend that it be accepted as fulfilling the dissertation requirement for the Degree of Doctor of Philosophy.

Nasser Peyghambarian	Date 4/18/91
Dror Sarid	Date 4/17/91
Neal R. Armstrong	Date 4/17/91
Sumit Mazumdar	Date 4/17/91
Markus Lindberg	Date 4/18/91

Final approval and acceptance of this dissertation is contingent upon the candidate's submission of the final copy of the dissertation to the Graduate College.

I hereby certify that I have read this dissertation prepared under my direction and recommend that it be accepted as fulfilling the dissertation requirement.

Dissertation Director	Date 4/18/91

STATEMENT BY AUTHOR

This dissertation has been submitted in partial fulfillment of requirement for an advanced degree at The University of Arizona and is deposited in the University Library to be made available to borrowers under rules of the Library.

Brief quotations from this dissertation are allowable without special permission, provided that accurate acknowledgment of source is made. Requests for permission for extended quotation from or reproduction of the manuscript in whole or in part may be granted by the head of the major department or the Dean of the Graduate College when in his or her judgment the proposed use of the material is in the interests of scholarship. In all other instances, however, permission must be obtained from the author.

SIGNED: Valorie S. Williams

TABLE OF CONTENTS

Page

LIST OF ILLUSTRATIONS

Page

ABSTRACT

The history of femtosecond laser pulse generation is summarized and a current state-of-the-art femtosecond laser system described. The femtosecond pulses are used to observe coherent coupling effects in a fluoro-aluminum phthalocyanine thin film. The polarization dependency of the coherent coupling indicates that orthogonal polarization states in the phthalocyanine ring are effectively uncoupled. The coherent coupling effect evolves into a nonequilibrium exciton population spectrally coincident with the pump pulse. This population rapidly decays to the bottom of the π-π^* absorption band. These singlet excitons exhibit rapid bimolecular decay characteristics. In addition, some singlet excitons relax into the triplet manifold by intersystem crossing. Excited-state triplet-triplet absorption is then observed. The triplet excitons relax to the ground state, apparently via nonradiative decay mechanisms.

Femtosecond techniques are also employed to demonstrate a picosecond all-optical organic NOR gate. A dye-doped polymer is used as the nonlinear material inside a Fabry-Perot etalon.

CHAPTER 1

INTRODUCTION

Nonlinear optical processes are the fundamental tools for future photonics technologies, such as optical signal processing, optical computing, image processing, and optical frequency conversion. The advantages of photonics over electronics are gain in bandwidth and three-dimensional interconnectivity. To realize these advantages, it is necessary to understand the basic physical mechanisms of nonlinear optical phenomena. Fundamental research in nonlinear optics deals with the physics of optically-nonlinear interactions, the dynamics of photo-excited electrons, and the microscopic relationship between the chemical and physical structure of a material and its nonlinear optical properties.

In general, the optical response of a material is a measure of the electric dipole moment, or polarization, P, induced in the material by an oscillating optical radiation field. When the applied field is strong, i.e. an intense laser pulse, the electric dipole interaction with the radiation shows a nonlinear behavior. The polarization can be expressed as a Taylor series expansion [Shen (1984)]:

$$P = \chi^{(1)}.E + \chi^{(2)}:EE + \chi^{(3)}\vdots EEE + \ldots$$

where E is the incident electromagnetic field, $\chi^{(1)}$ is the linear susceptibility, and $\chi^{(2)}$ and $\chi^{(3)}$ are the second and third order susceptibilities.

Materials with large $\chi^{(2)}$ coefficients are useful for second harmonic generation, or frequency doubling, and for the Pockel's electro-optic effect where the refractive index of a material is modulated by a low-frequency electric field. Typical second-order devices are electro-optic spatial light modulators and electro-optical switches. Materials with large $\chi^{(3)}$ coefficients are useful for third harmonic generation, or frequency tripling, and for applications requiring an intensity-dependent refractive index, such as optical

communications and optical signal processing. Here, an intensity-dependent phase shift is induced in a nonlinear material by the intensity-dependent refractive index. This, in turn, changes some parameter of the device, i.e. the coupling angle into a waveguide or the resonance cavity length of a Fabry-Perot etalon. Unlike second order optical nonlinearities, which are only observed in materials with no center of symmetry, third order optical nonlinearities are observed to some degree in all materials.

Nonlinear optical materials can be roughly divided into three classes: organic molecular crystals, organic polymers, and inorganic crystals. In molecular crystals, molecular units are bonded by weak van der Waals forces. The optical nonlinearities are attributed to the electronic structure of the individual chemically-stable and separable constituent molecules. In organic polymers and inorganic crystals, atomic units are bonded by covalent or ionic forces resulting in a bulk system. The optical nonlinearities are derived from the electronic properties of the bulk material as opposed to the constituent molecules.

In inorganic crystals, electrons are excited from the valence band into the conduction band by an external optical field. The resulting many-body electronic interactions contribute to the optical nonlinearity. In organic systems, the main contribution to the optical nonlinearity is photo-induced distortion of the conjugated π-electron systems. In organic polymers, the conjugated π-electron system is modified by the migration of photo-excited electrons between atomic units within the π-electron system. In molecular crystals, the π-electron system of the molecular unit is perturbed by an external optical field. The optical field excites the molecular π-electron system from its ground state to an excited state. In some cases, this "excitation" can then migrate between molecular units of the crystal. Larger nonlinear responses have been measured for organic polymers which contain larger numbers of conjugated π-electrons per unit volume [Neher *et. al.* (1990)]. While inorganic

semiconductors have been widely studied for many years, the study of organic systems is relatively recent.

Sixteen years ago, electronic coupling between π-electron systems of the benzene ring and various radicals was discussed as a fundamental mechanism responsible for the large nonlinear coefficients in benzene substitutes [Oudar and Chemla (1975)]. One year later, the large optical nonlinearity in polydiacetylene polymers was attributed to delocalization of the conjugated π-electrons along the polymer backbone [Sauteret *et. al.* (1976)]. A later theoretical development indicated that the nonlinear coefficients in conjugated polymers increase with increasing π-electron delocalization [Agrawal *et. al.* (1978)]. Current microscopic theories also predict that conjugated π-electrons induce large non-resonant third-order optical nonlinearities [Prasad (1988)]. The largest organic third order nonlinear effects have been observed in pseudo-one-dimensional crystalline polydiacetylenes [Carter *et. al.* (1985), Chemla and Zyss (1987)]. In fact, the nonresonant $\chi^{(3)}$ of organics is often comparable to or larger than that for inorganics [Sauteret *et. al.* (1976), Ho *et. al.* (1986)]. In addition, the non-resonant nonlinearities in organic materials respond on a femtosecond time scale [Carter *et. al.* (1986), Carter (1987), Prasad (1988)]. Since the nonresonant third-order optical nonlinearities are large and exhibit rapid response times, nonlinear organic materials are of considerable scientific interest.

Optically-nonlinear organics are available as single crystals, Langmuir-Blodgett films, nonlinear molecules doped in polymer hosts, side chain polymers, sublimed thin films, etc. A basic understanding of the microscopic nonlinear mechanisms in these materials will permit chemists to synthesize organic structures which enhance optical nonlinearities for specific device applications. Many organic polymers are soluble and thus can be processed into fibers and films. Since these polymers can also have large nonresonant third order

optical nonlinearities, they may soon be able to compete with the usual inorganic nonlinear materials for use in integrated nonlinear optical devices.

While understanding the physical origin of the microscopic optical nonlinearities in organics is essential for their use in nonlinear optical devices, for high-speed optical communications and signal processing applications it is equally important to understand and time-resolve the ultrafast dynamics of the photo-excited states in these materials. These dynamics may be significantly affected when the nonlinear molecules of the material are placed within van der Waals distances. Femtosecond optical measurement techniques provide a means of directly observing the temporal evolution of nonlinear optical processes. In particular, ultrashort pump-probe spectroscopy has emerged as an important method for studying excited-state dynamics. The femtosecond laser facility, which generates ultrashort femtosecond pulses is reviewed in Chapter 2. In addition, the experimental setup for the transient pump-probe spectroscopy experiments used to characterize organic phthalocyanine materials and to demonstrate an organic all-optical etalon switch is discussed in Chapter 2.

The two-dimensional, planar phthalocyanines (Pcs) are good organic candidates for nonlinear optical devices as they exhibit picosecond excitonic lifetimes, chemical and thermal stability, and relatively large third order optical nonlinearities. It was first thought that the third order nonlinearity in one-dimensional conjugated π-electronic systems would increase continuously with chain length. Recent studies on polyphenyls and polythiophenes have shown, however, that $\chi^{(3)}$ actually saturates at a finite chain length [Zhao *et. al.* (1988), Zhao *et. al.* (1989)]. The third order optical nonlinearity in conjugated organic linear chains, such as polyenes, was found to have a power law dependence on chain length [Heflin *et. al.* (1988)]. The saturation of $\chi^{(3)}$ as a function of chain length was recently explained microscopically for *trans*-polyacetylene and polydiacetylene [Dixit *et. al.* (1991)]. The bulk

of the nonlinearity was found to be determined by contributions from only two channels regardless of chain length. As more atoms are added to the conjugated polyene, the number of possible channels increases rapidly. The two dominant channels, however, simply approach their asymptotic values and the additional terms make only small contributions to $\chi^{(3)}$. It is possible that finite two-dimensional conjugated π systems may exhibit additional interesting and desirable nonlinear optical properties.

Pcs are aromatic molecules with large two-dimensional π-electron systems which lead to intense absorption bands at 400 and 700 nm. They exhibit relatively large third order nonlinearities for organic materials. A nonresonant $\chi^{(3)} = 5\text{x}10^{-11}$ esu has been measured for polycrystalline FAlPc thin films from third harmonic generation measurements [Ho *et.al.* (1987)]. "Effective" resonant $\chi^{(3)}$ values of $\approx 2\text{x}10^{-9}$ esu and $\approx 3\text{x}10^{-9}$ esu have been reported in degenerate four wave mixing studies on Langmuir-Blodgett films of silicon Pc [Casstevens *et. al.* (1990)] and metal-free tetrakis cumylphenoxy Pc ($H_2Pc(Cp)_4$) [Prasad (1988b)], respectively. These values are comparable to $\chi^{(3)}$ values measured for one-dimensional polymeric polyacetylene and polydiacetylene [Sauteret *et. al.* (1976), Carter *et. al.* (1985), Chemla and Zyss (1987), Kajzar *et. al.* (1987, 1988)].

In addition, subpicosecond and picosecond time-scale excitonic decay components have been measured in thin films of FAlPc [Ho and Peyghambarian (1988)] and $H_2Pc(Cp)_4$ [Prasad (1988b)]. This is much faster than the nanosecond time-scale electron-hole recombination lifetime observed in bulk inorganic semiconductors but similar to decays observed in small inorganic semiconductor microcrystallites [Williams *et. al.* (1988)]. Presumably, two factors contribute to the rapid decay observed in Pc thin films and size-confined inorganic crystals: localization of the excitation and efficient nonradiative decay. In Pcs, the excitation remains localized on some Pc molecule; the excited electronic orbital

configuration can rapidly relax back to the ground configuration. In confined crystals, the electron does not travel far from its geminate hole, thus electron-hole recombination is efficient. In bulk inorganic crystals, the electron is free to travel throughout the crystal lattice. Nonradiative decay is probably the dominant contribution to rapid decay. Rapid nonradiative decay through surface states has been identified in confined crystals [Williams *et. al.* (1988)]. In Pc thin films, efficient nonradiative decay occurs due to coupling between adjacent molecules. In addition to relatively large, rapid nonlinearities, Pcs also exhibit interesting semiconductivity and photoconductivity properties [Popovic (1984), Klofta *et. al.* (1985), Simon and André (1985) pp. 103-149, Laurs and Heiland (1987)]. The intrinsic conduction energy band gap in Pcs is 2.0 eV [Simon and André (1985) p.105]. Thus, Pcs are particularly interesting organic materials for optical study.

Chapter 3 reviews the properties of phthalocyanine molecules and aluminum phthalocyanine thin films. Ultrafast polarization-dependent spectral hole burning observed in a fluoro-aluminum phthalocyanine thin film is presented in Chapter 4. Chapter 5 reviews the relaxation dynamics of phthalocyanine solutions and thin films, and Chapter 6 presents the dynamics of absorption saturation and induced absorption in aluminum phthalocyanine thin films. A picosecond all-optical organic etalon switch constructed from a composite dye-doped polymer is demonstrated in Chapter 7. Chapter 8 concludes the manuscript with possible future research directions.

CHAPTER 2

FEMTOSECOND LASER FACILITY

The femtosecond laser facility consists of a colliding-pulse mode-locked ring dye laser (CPM) which produces ≈60 fs laser pulses. The pulses are intensified using one or two amplifiers and split into two beams for performing pump-probe transient spectroscopy experiments.

Colliding-Pulse Mode-Locked Ring Dye Laser

Ultrashort CPM pulses are produced by passively mode-locking a continuous wave (cw) ring dye laser. Every laser has two primary components: gain and feedback. The gain is realized by creating a population inversion in a medium either electrically or optically. The feedback is realized by using two or more mirrors to form either a linear or ring cavity. When the gain in the optical cavity exceeds the losses of the cavity, an electromagnetic field oscillates inside the cavity. The gain for a cw dye laser is provided by an optically-pumped (i.e. laser or flashlamp pumped) gain dye. A cw dye laser can be passively mode-locked to produce a train of short light pulses by placing a saturable absorber inside the laser cavity. The duration of the pulses is inversely proportional to the oscillating bandwidth of the gain dye, and the pulses are separated by the round-trip cavity time. The absorption coefficient of a mode-locking saturable material is constant at low light intensities but saturates and becomes lower at higher intensities.

Following Siegman's description in *Lasers*, the build up of a passively mode-locked pulse from noise can be explained as follows. Sometime after the laser pumping mechanism is turned on, the gain builds up such that the gain in the cavity exceeds the losses. At this point, weak noise oscillations begin to build in the cavity. As these oscillations circulate

repeatedly around the cavity, the largest noise spike becomes amplified such that it eventually saturates the absorber. This spike then experiences less loss per round trip thus increasing its amplitude even further relative to the other noise spikes. The noise spike continues to be amplified until it eventually saturates the gain such that no other noise oscillations are amplified. In this manner, the noise spike becomes a single, short laser pulse traveling around the cavity.

The temporal width of the pulse, τ_p, is shortened by each transmission through the saturable absorber. When τ_p is much shorter than the absorption recovery time of the saturable absorber, T_1, as is the case for the CPM laser where $\tau_p \lesssim 100$ fs and $T_1 \approx 100$ ps,

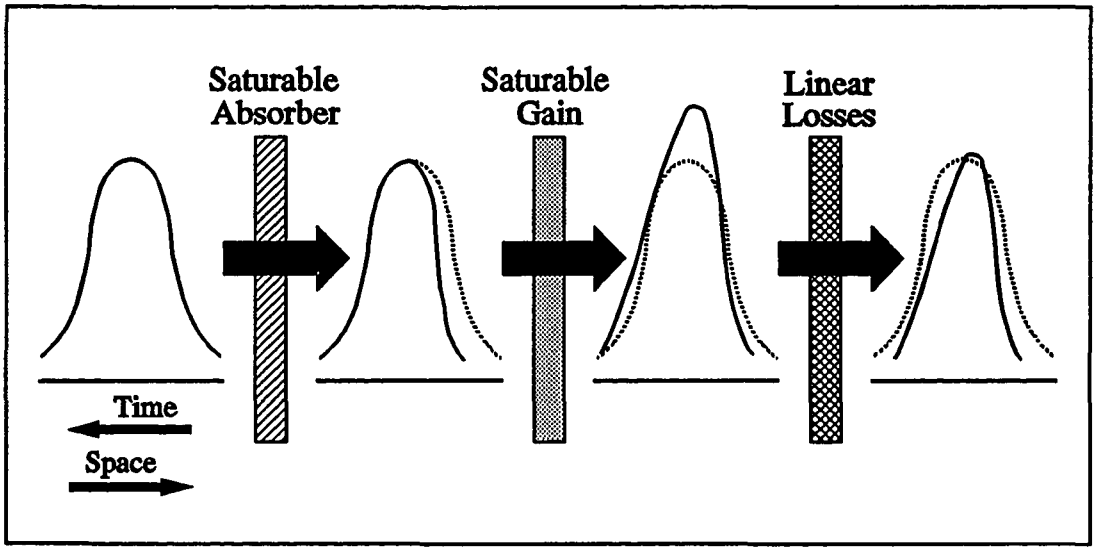

Figure 2.1 Pulse shortening mechanism

the pulse shortening mechanism can be visualized as shown in Figure 2.1. The low intensity leading edge of the pulse is absorbed by the saturable absorber. As the more intense central portion of the pulse travels through the absorber, the integrated intensity, or energy of the pulse saturates the absorber thus allowing the remaining portion of the pulse to pass. When

the pulse travels through the gain dye, the energy of the pulse saturates the gain and the trailing edge of the pulse experiences less gain. In this manner, the leading and trailing edges of the pulse are truncated resulting in shorter pulses.

This pulse shortening mechanism is limited by the spectral bandwidth (BW) of the cavity and group velocity dispersion (GVD). According to Fourier transform theory, $\Delta\upsilon\Delta t \sim 1$, limiting the spectral BW of the pulse necessarily increases the temporal width of the pulse. The BW in the cavity is limited by the gain and absorber dyes and the mirror coatings. While metal mirrors have broadband reflectivity as required for ultrashort pulses, their reflection losses can vary from 5 to 40% [Knox *et. al.* (1988)]. Dielectric coatings can decrease the reflection losses while maintaining a broad BW, but they also increase GVD. Single stack dielectric coatings have been found to be the best compromise (adequate BW with minimum GVD). GVD results from the fact that different wavelengths travel through dispersive media at different velocities resulting in a modification of the relative phases within the pulse. GVD is induced by dispersion in the mirror coatings, as well as in the dye solvents and glass components. Bandwidth-limiting and GVD, which are linear phenomena, both broaden the pulse envelope. The pulse shortening mechanism can be enhanced by balancing these linear effects with the nonlinear self-phase modulation effect as will be discussed below.

History of the mode-locked *linear* dye laser

The first reported passive mode-locking of a cw dye laser used Rhodamine 6G dye as the gain medium and diethyloxadicarbocyanine iodide (DODCI) as the saturable absorber inside a linear laser cavity [Ippen *et.al.* (1972)]. The Rhodamine 6G was pumped with a cw argon laser producing a stable mode-locked train of 1.5-ps full width at half maximum (FWHM) pulses. (FWHM is to be understood in all future references to pulse duration.) The

mode-locking wavelength was tunable over a 20-nm range on the long wavelength side of both the gain and absorber curve peaks. Both dyes were circulated to prevent the high intensities of the pulses from instantly destroying the dyes.

This first passively mode-locked cw dye laser, developed at Bell Telephone Laboratories (Bell Labs), underwent several modifications and additions as it matured into the current state-of-the-art CPM laser. The Bell Labs researchers were soon able to generate subpicosecond (500 fs) pulses by mixing the Rhodamine 6G and the DODCI together in a single solution [Shank and Ippen (1974)]. Returning to the separate Rhodamine 6G and DODCI configuration and using an autocorrelation technique (discussed below), the Bell Labs researchers observed a nonlinear frequency chirp in the optical pulses which swept from red to blue in time resulting in an asymmetric pulse spectrum [Ippen and Shank (1975)]. By sending the pulses through a grating pair, to remove the linear component of the chirp, and then spectrally filtering the pulse, they obtained 300-fs bandwidth-limited pulses.

A group from Imperial College produced 300-fs bandwidth-limited (chirp-free) pulses directly from the laser cavity by placing the DODCI saturable absorber cell in contact with the high reflectivity cavity mirror and placing a tuning prism in the cavity. [Ruddock and Bradley (1976)]. From their results, they deduced a hyperbolic secant intensity profile as expected for bandwidth-limited pulses. The hyperbolic secant solution for cw mode-locked pulses can be fairly easily derived [Haus (1975), Haus *et. al.* (1975), Siegman (1986)]:

$$I(t) = I_0 \operatorname{sech}^2 \left[\frac{1.763t}{\tau_p} \right].$$

$I(t)$ is the instantaneous intensity of the pulse, t is time, τ_p is the FWHM of the pulse, and $I_0(t)$ is the peak intensity.

History of the mode-locked *ring* dye laser

It took five years to realize the next important refinement of the mode-locked dye laser: the ring cavity. The Bell Labs researchers produced 90-fs pulses in a ring cavity by colliding two synchronized counter-propagating pulses in the saturable absorber [Fork *et. al.* (1981)]. They coined this process "colliding pulse modelocking (CPM)", an expression still commonly used. The Rhodamine 6G gain dye jet and the DODCI absorber dye jet were separated by one-quarter of a round trip path length. The gain was pumped with all six lines of a cw argon laser. The counter-propagating pulses synchronize since minimum energy loss occurs when the two pulses arrive at the saturable absorber simultaneously. The collision of the two pulses in the saturable absorber enhances the pulse shaping effects of the absorber. The leading edges of both counter-propagating pulses help to bleach the absorber allowing the remainder of each pulse to pass. In addition, the pulses create a transient population grating in the DODCI molecules. The trailing edge of one pulse can scatter off the population grating into the center of the pulse travelling in the other direction, and constructive interference between the original and scattered pulses can make the absorber appear more transparent [Dietel (1982)]. The result is a stabilized train of ultrashort pulses.

At this point, the Bell Labs researchers were able to produce 30-fs pulses by sending amplified CPM pulses [Fork *et. al.* (1982)] through a short optical fiber and compressing the resulting spectrally-broadened, chirped pulses with a grating pair [Shank *et. al.* (1982)]. Our fiber-grating pulse compression system is discussed below.

It was soon observed that the CPM pulses could be shortened by placing a glass prism inside the CPM cavity [Dietel *et. al.* (1982)]. Since low frequencies travel through glass faster than high frequencies (positive GVD), this indicated that the pulses generated directly from the CPM laser exhibited a pronounced frequency down-chirp, that is, the high-frequency components occurred in the leading edge of the pulse and the low-frequency components in

the trailing edge. This description of chirp is strictly valid only within the slowly-varying-envelope approximation. The glass prism allowed the trailing edge of the pulse to catch up to the leading edge thus balancing the GVD in the ring [Dietel *et. al.* (1983)].

Refining this idea, the Bell Labs researchers inserted a four-prism assembly into the CPM cavity [Fork *et. al.* (1984)] as shown in Figure 2.2. The low-frequency components

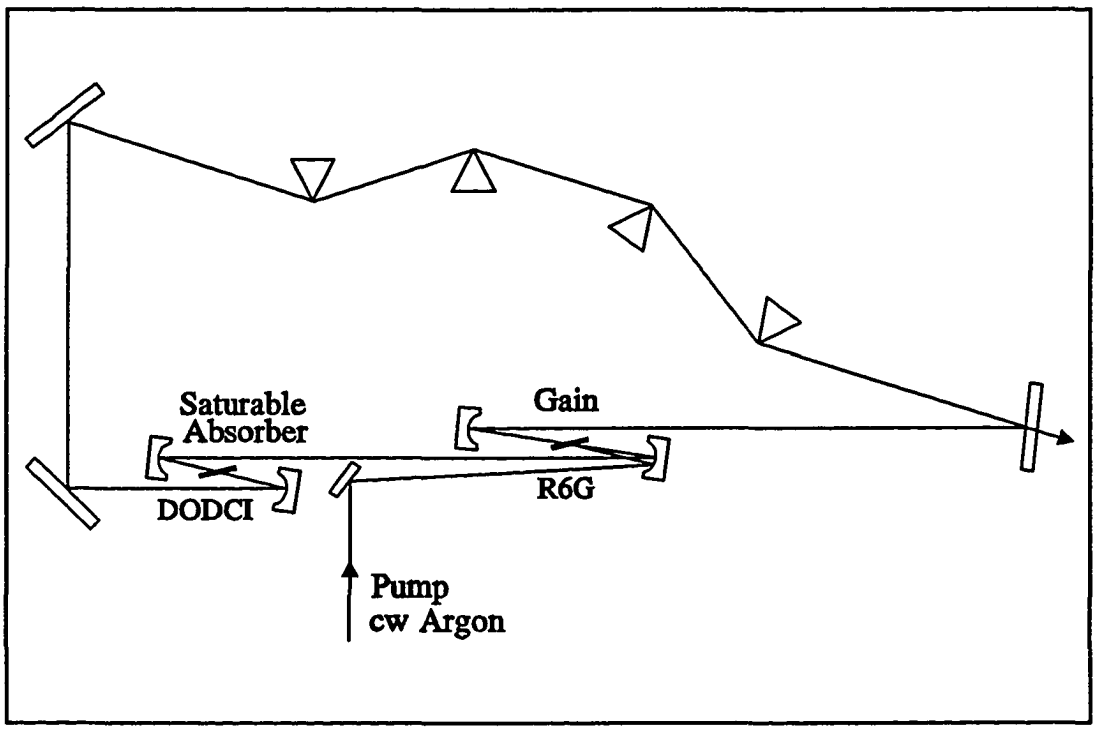

Figure 2.2 Colliding-pulse mode-locked (CPM) ring dye laser

travel through the first prism faster than the high-frequency components (positive GVD). In addition, the prism diffracts the high frequencies through a larger angle. The high frequencies thus travel a farther distance to the next prism resulting in additional positive GVD in the region between the prisms. At the second prism, however, the low frequencies are then forced to travel through a thicker section of the prism than the high frequencies.

If the distance between the prisms is sufficiently large, the high frequencies traverse the prism pair in a shorter time than the low frequencies resulting in a net negative GVD. The second prism pair recombines the spatially separated frequency components as well as adding to the cumulative GVD. For properly spaced prisms, translating any prism perpendicular to its base allows the GVD be adjusted continuously from positive to negative values. The transmitted beam remains collinear with the incident beam throughout the adjustment. In addition, using the prisms at Brewster's-angle incidence minimizes reflection losses.

The Bell Labs researchers also noticed the similarities between soliton propagation in optical fibers and pulse shaping in passively mode-locked lasers [Martinez *et. al.* (1984)]. They showed, theoretically, that balancing GVD and self-phase modulation inside the optical cavity could reduce the pulse duration. As discussed above, reflection of the pulse from the dielectric mirrors and dispersion in the dye solvents and prisms induce positive GVD. Self-phase modulation is a nonlinear phenomena which causes a frequency sweep (from low to high frequencies in time) and generates new frequencies in the pulse [Alfano and Ho (1989)]. It occurs when the high intensity CPM pulses propagate through a medium producing a nonlinear change in the refractive index of the dye solvents. Since new frequencies are generated, the pulse width can be reduced below the limit set by the gain BW. By carefully balancing the positive GVD, self-phase modulation frequency sweep, and negative GVD introduced by the four-prism assembly, a shortening of the pulse can be realized. The Bell Labs researchers demonstrated this balancing experimentally by obtaining 27-fs, 620-nm pulses at a 95-MHz repetition rate directly from the CPM laser [Valdmanis *et. al.* (1985)]. These are the shortest pulses generated directly from a laser oscillator to date. (Pulses as short as 6 fs, or three optical cycles, have been obtained using a fiber-grating compressor external to the CPM cavity [Fork *et. al.* (1987)].)

The Bell Labs researchers also noticed the similarities between soliton propagation in optical fibers and pulse shaping in passively mode-locked lasers [Martinez *et. al.* (1984)]. They showed, theoretically, that balancing GVD and self-phase modulation inside the optical cavity could reduce the pulse duration. As discussed above, reflection of the pulse from the dielectric mirrors and dispersion in the dye solvents and prisms induce positive GVD. Self-phase modulation is a nonlinear phenomena which causes a frequency sweep (from low to high frequencies in time) and generates new frequencies in the pulse [Alfano and Ho (1989)]. It occurs when the high intensity CPM pulses propagate through a medium producing a nonlinear change in the refractive index of the dye solvents. Since new frequencies are generated, the pulse width can be reduced below the limit set by the gain BW. By carefully balancing the positive GVD, self-phase modulation frequency sweep, and negative GVD introduced by the four-prism assembly, a shortening of the pulse can be realized. The Bell Labs researchers demonstrated this balancing experimentally by obtaining 27-fs, 620-nm pulses at a 95-MHz repetition rate directly from the CPM laser [Valdmanis *et. al.* (1985)]. These are the shortest pulses generated directly from a laser oscillator to date. (Pulses as short as 6 fs, or three optical cycles, have been obtained using a fiber-grating compressor external to the CPM cavity [Fork *et. al.* (1987)].)

This type of CPM laser (Fig. 2.2) was used to generate the femtosecond pulses used in the experiments to be discussed in this manuscript. In our CPM laser, we use single-stack dielectric mirrors with a maximum reflectance at 620 nm. Each of the three mirrors has two outputs. The low-intensity outputs of the two high reflectivity mirrors are used for triggering, monitoring the temporal and spectral widths of the pulse, and observing the mode quality. The high power outputs are used for the experimental pulse train and for power metering. We employ a 375-μm stainless steel laser dye jet for the Rhodamine 6G and a

10-μm jet for the DODCI. Steady dye flow is provided by stabilized dye circulators [Beisser (1981), Olbright (1987)]. The Rhodamine 6G is pumped with all six lines of an s-polarized cw argon ion laser and the dye jets and prisms are aligned at Brewster's angle. This results in nominally s-polarized pulses. We typically obtain pulse durations of $\approx$60 fs. The pulse width and wavelength of the pulses ultimately depend on the age of the DODCI.

Autocorrelation

Since conventional detection systems have, at best, picosecond time resolution, the pulse widths are measured using a nonlinear optical technique called autocorrelation.

Background-free intensity autocorrelator

Background-free autocorrelation [Ippen and Shank (1975)] is illustrated in Figure 2.3. The pulse to be measured is beamsplit into two separate pulses. After traversing separate delay arms, both beams are focused to a common spot on a nonlinear, second-harmonic,

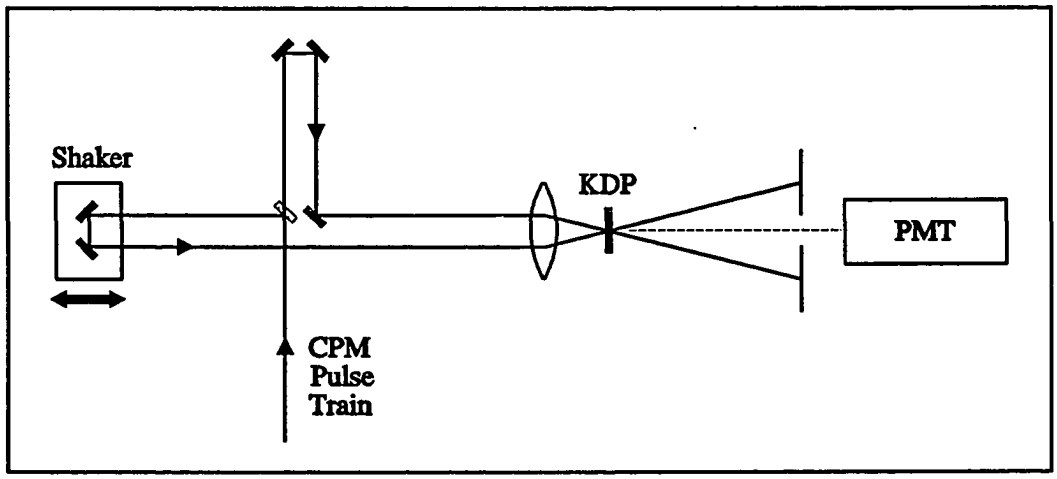

Figure 2.3 Background-free autocorrelator

100-μm thick potassium dihydrogen phosphate (KDP) crystal. The thinness of the crystal broadens its phase-matching condition allowing the entire BWs of the pulses to be

upconverted. A small angle separates the two beams spatially. The path length of one of the beams is varied with an electronic shaker thus changing the time delay of that pulse. A phase-matching condition of the crystal is met at the bisector of the angle separating the two beams when the beams are temporally and spatially overlapped. As one pulse is swept over the other pulse in time at the crystal, a sum-frequency signal is generated at the bisector angle which corresponds to the autocorrelation of the temporal profile of the original pulse.

The sum-frequency autocorrelation signal is proportional to the product of the intensities of the two pulses and spatially separated from the second-harmonic signals generated by each individual beam. This allows the autocorrelation signal to be monitored separately from the individual second-harmonic (SH) signals (background-free detection) with a photomultiplier tube (PMT) connected to an oscilloscope. As one pulse sweeps back and forth across the other, the autocorrelation trace is monitored on the oscilloscope. A blanking circuit allows only the signal generated by the sweep in one direction to be observed. By monitoring the autocorrelation signal *in situ*, the prisms in the CPM cavity can be adjusted for minimum pulse width. The autocorrelation

$$\int_{-\infty}^{\infty} \mathrm{sech}^2(\tau)\,\mathrm{sech}^2(\tau-t)\,d\tau = \frac{3[\tau\cosh(\tau)-\sinh(\tau)]}{\sinh^3\tau}$$

has a FWHM of 2.720 [Diels *et. al.* (1985)]. A $\mathrm{sech}^2(t)$ pulse has a FWHM of 1.763. Thus, the temporal width of the CPM pulses is computed by dividing the measured autocorrelation FWHM by the deconvolution factor for a $\mathrm{sech}^2(t)$ pulse shape, 2.720/1.763=1.543. GVD in the KDP crystal can cause the measured pulse width to be as much as 5 fs broader than the actual CPM pulse width [Shank *et. al.* (1982)].

Collinear interferometric autocorrelator

A collinear interferometric autocorrelator, illustrated in Figure 2.4, can also be used to measure pulse width [Diels *et. al.* (1985)]. The interferometric autocorrelator operates

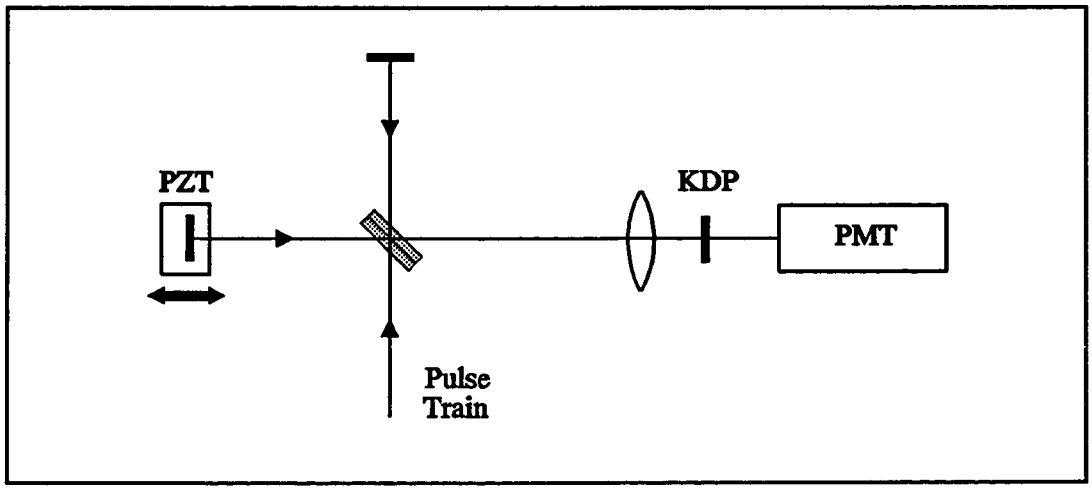

Figure 2.4 Interferometric autocorrelator

similar to the background-free autocorrelator except that the two beams are recombined collinearly. A piezo-electric transducer (PZT) is used to vary the time delay. A 30-μm thick KDP crystal is used for second harmonic conversion. The thinness of the crystal minimizes GVD-induced pulse duration errors and prevents BW-limiting of the SH signals. A PMT monitors the interference SH signal between the two pulses as well as both individual SH signals. The interference signal retains useful phase information which is lost using the background-free method. This technique, however, is extremely sensitive to vibrations. As our experiment table is not isolated from vibrations, we did not obtain useful results using this technique. It is important to use this collinear technique when measuring very short pulses, i.e. less than 15 fs, since pulse width measurements yield slightly longer values when a small tilt exists between the pulse trains. For longer pulses, the few fs error is not significant.

Bow-Tie Amplifier

The 620-nm, 95-MHz, 60-fs pulses generated from our CPM laser have nominal pulse energies of ≈150 pJ. In general, these ≈2 kW pulses do not have high enough peak intensities to observe nonlinear optical phenomena. Therefore these pulses are amplified. By focusing amplified pulses onto a sample, the nonlinear properties can be studied by observing the changes induced in the transmission spectrum of the sample. Amplified pulses are also used to generate continuum pulses such that the changes induced in the sample can be monitored over a broad BW. In addition, amplified pulses allow us to obtain tunability. These points will be discussed in detail below.

Pulses with gigawatt powers and 10-Hz repetition rates were first achieved using a multi-stage amplifier pumped with the doubled output of a Q-switched Nd^{+3}:yttrium aluminum garnet (YAG) laser [Fork *et. al.* (1982)]. The 400-fs pulses exiting the amplifier were reduced to 70 fs using a grating compressor but suffered from poor beam quality and focusability due to the transverse pumping geometry. The Bell Labs researchers later produced 100-fs (after grating compression), 10-GW/cm^2 pulses at 5-kHz using a 6-pass bow-tie amplifier pumped with a copper vapor laser (CVL) [Knox *et. al.* (1984)]. The increased repetition rate results in higher signal-to-noise ratios and improved detection sensitivity in signal averaging experiments. In addition, good beam quality was preserved in this amplifier. The amplified pulses were therefore focusable to within 10 percent of the diffraction limit resulting in higher peak intensities than obtainable with multi-stage amplifiers. The amplification efficiency (pump energy transferred to the pulse) is about 10^{-2} for all femtosecond amplifiers designs [Knox (1988)].

The six-pass bow-tie amplifier used to intensify our CPM pulses, illustrated in Figure 2.5, is based on this Bell Labs configuration. The gain medium, sulforhodamine 640 dissolved in ethylene glycol (EG), is circulated through a dye cell. A CVL beam, focused

to about 1 mm in diameter, is used to generate a population inversion in the gain dye. Gas discharge CVL's are not typical lasers. There is no feedback or build up of stimulated emission in the laser cavity. CVL pulses are produced by "brute force" lasing action. Basically, a large population inversion is created in the copper atoms by collisions with an excited buffer gas, neon. The neon is charged by a pulse of high voltage applied between the anode and cathode of the laser tube using a thyratron device. The neon excitation is transferred to the copper atoms by collisions. The copper atoms then radiate into two metastable states yielding a discharge pulse with 510 nm and 578 nm radiation. After the metastable states relax to the ground state via electron impact and wall collisions, the thyratron can be fired again to produce another pulse. The typical, 25-ns, randomly-polarized CVL pulse consists of a small superradiance peak on the leading edge of the pulse, a main lasing peak corresponding to the firing of the thyratron, then several smaller subsidiary peaks corresponding to reflections of the main peak off the back cavity mirror.

As the CPM pulses are nominally s-polarized as discussed above, p-polarized CVL pump radiation merely induces amplified spontaneous emission (ASE) and heating of the dye solvent and cell, and does not contribute to the amplification of the CPM pulses. We place a polarizing beamsplitter cube in the CVL output beam to eliminate the undesirable p-polarized light from the randomly polarized beam. By delaying the reflected p-polarized beam and reflecting it back into the cavity, shorter pulse widths ($\approx$15 ns) are obtained though half the power is lost. The separated p-polarized mode is trapped i.e. it cannot escape from the cavity. The trapped beam is delayed such that when it is sent back into the cavity, the gain is depleted for the second subsidiary peak of the pulse thus preventing the rear end of the pulse from oscillating [Nighan (1991)]. The result is a shorter pulse.

The CPM pulses are directed through the gain dye coincident with the focused CVL on six separate passes producing an average gain of ≈6 per pass. The gain achieved by the fifth and sixth passes is smaller due to depletion of the population inversion by earlier passes.

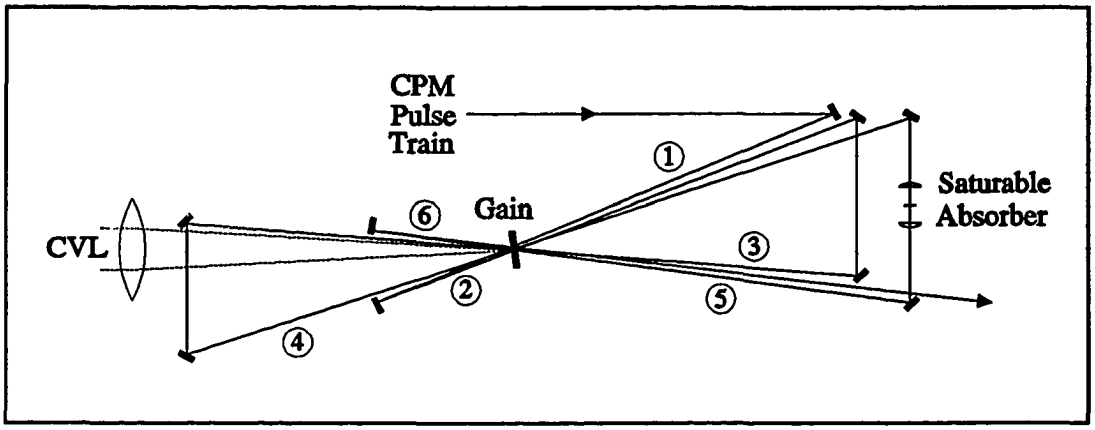

Figure 2.5 Bow-tie amplifier

The CVL laser is triggered by the CPM pulses (detected by a fast photodiode and frequency down converted to 8.5 kHz) and delayed with a Stanford pulse generator such that a CVL pulse arrives at the gain dye simultaneously with a CPM pulse. Because the CVL operates at 8.5 kHz, approximately every 11,000th CPM pulse is amplified. Since the CPM pulses are separated by only ≈11 ns (95-MHz repetition rate), it is important to keep the CVL pulses short enough such that the pulses adjacent to the amplified CPM pulse do not become amplified as well. The amplified CPM pulses are focused onto a thin circulating jet of saturable absorber (Malochite Green dissolved in EG) between the fourth and fifth passes to absorb ASE and unamplified pulses. Since Malochite Green has a picosecond absorption recovery time, it can absorb the nanosecond lifetime ASE which accompanies the amplified pulses.

The original Bell Labs bow-tie amplifier utilized several lenses and a gain dye jet. We found that by removing the lenses and placing the mirrors closer to the gain medium, we were able to reduce the induced GVD. In addition, we obtained a much improved beam quality by using a dye cell instead of a free-flowing dye jet. These modifications, while improving the gain efficiency, also increased the ASE resulting in feedback into the CPM cavity. The scattered ASE feedback was found to originate dominantly from the fourth pass where the ASE is at a maximum, just before the saturable absorber. We were able to suppress the feedback and thus maintain CPM stability by using the modified bow-tie configuration shown in Figure 2.5.

With ≈12 W of CVL power, a gain of approximately $5x10^4$ is achieved in our modified bow-tie amplifier resulting in ≈5 μJ per pulse at 8.5 kHz. Because of the GVD induced by the dyes, cell, and solvents, the pulses leaving the amplifier are considerably broadened. We send the amplified pulses through a prism assembly, similar to the one inside the CPM cavity, to compensate for the GVD. To reduce the number of prisms required for pulse compression, the initial pass through the prisms is reflected back through the same prisms at a different height. The resulting ≈100-fs FWHM, 620-nm, 15-nm BW, 8.5-kHz repetition rate, amplified pulses are then divided and used for pump-probe transient spectroscopy experiments where an intense "pump" pulse is used to excite the sample, and a weak "probe" pulse is used to probe the induced transmission changes.

Continuum Generation

It is often desirable to perform pump-probe spectroscopic experiments with a broadband probe pulse so that the pump-induced transmission changes of a sample can be studied over a broad wavelength region. A continuum can be generated by focusing an ultrashort pulse on a clear liquid i.e. water, EG, etc. A threshold of ≈10^{12} W/cm^2 is required

for a 1-mm thick jet of EG [Knox *et. al.* (1984)]. The continuum is generated dominantly by the self-phase modulation mechanism [Fork *et. al.* (1983)] as discussed above. While it is desirable to use thinner path lengths during continuum generation to reduce GVD in the probe pulse, the threshold intensity increases rapidly and the conversion efficiency diminishes as path length is reduced. We generate continuum probe pulses by focusing our amplified pulses to $\approx 5 \times 10^{12}$ W/cm^2 (well above threshold) with a microscope objective onto a 1-mm thick circulating EG jet yielding ≈450-850 nm BW pulses. The high intensity of the pump pulse can induce instabilities in the EG causing the continuum pulses to be noisy in the 620-nm region.

Fiber-Grating Pulse Compressor

In some cases, it is desirable to generate continuum pulses using a fiber-grating pulse compressor. A fiber-grating compressor, illustrated in Figure 2.6, can reduce the temporal

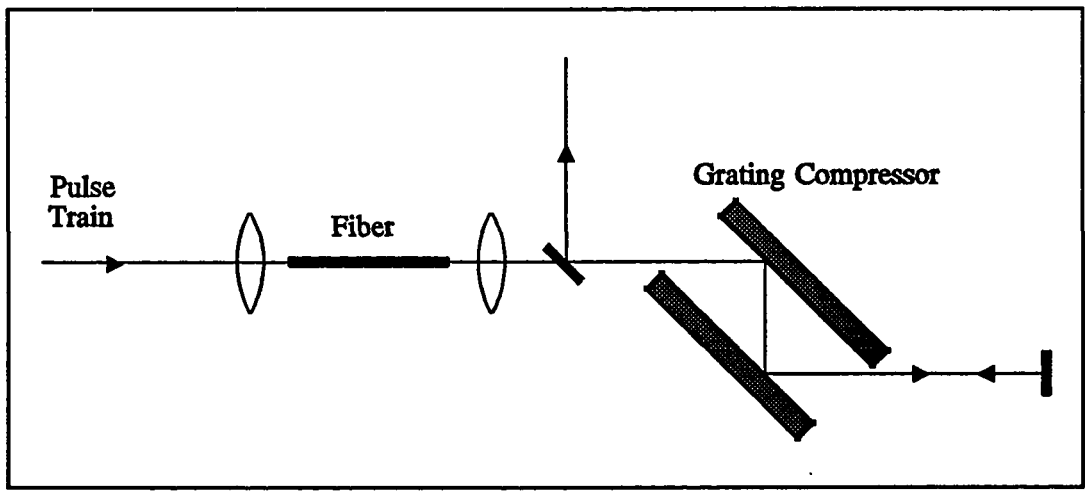

Figure 2.6 Fiber-grating pulse compressor

width and increase the BW of the pulses by a factor of ≈4. The shortest pulses obtained to date, 6 fs, or three optical cycles, were obtained using a fiber-grating compressor [Fork

et. al. (1987)]. In our pulse compression system, the amplified pulses are coupled into the 4-μm core of an ≈10-mm long single-mode optical fiber with a microscope objective. A frequency sweep, or chirp, is introduced into the pulse spectrum by nonlinear self-phase modulation and GVD as the pulse travels through the fiber. The spectrally- and temporally-broadened pulse is recollimated with another microscope objective and sent through a grating compressor [Treacy (1969)] which acts as a dispersive delay line. The grating compressor consists of two 600-line/mm gratings separated by ≈5 mm. The pulse is directed through the grating pair a second time at a different elevation to eliminate spatial distortion of the pulse, and the separation between the gratings is varied to minimize the pulse width. The grating compressor compensates for the chirp introduced by the fiber resulting in a "compressed" ≈25 fs broadband pulse. See Gomes *et. al.* (1988) for a complete review of fiber-grating pulse compression.

For the experiments discussed in this manuscript, we were interested in probing large wavelength regions of the sample. Since the largest BW obtained from our fiber-compressor, ≈60 nm, is narrow relative to the EG continuum BW, 400 nm, we obtained the data presented here using ethylene glycol continuum generation. These pump-probe experiments were performed at two different pump wavelengths: 620 nm and 760 nm. For 620-nm pump pulses, some of the amplified beam is split off before continuum generation. For 760-nm pump pulses, a portion of the continuum is split off for the probe beam, and the remainder is sent through an ≈10-nm BW, 780-nm interference filter tilted for 760-nm transmission. The 760-nm beam is then reamplified in a two-mirror telescopic amplifier pumped with a second CVL. This second amplifier permits the generation of tunable pump pulses.

Tunable-Pump Telescopic Amplifier

Femtosecond systems were at first restricted to studying materials which possessed optical absorbances at 620-nm or nonlinear phenomena inducible by the 620-nm CPM pulses. The ability to amplify other wavelength regions after continuum generation, thus realizing tunable pump pulses, has greatly increased the number of physical systems whose dynamics can be studied with fs pulses. Tunable fs pump pulses were first obtained at 10-Hz repetition rates using a multi-stage amplifier pumped with the doubled output of a YAG laser [Migus *et. al.* (1985)]. The portion of the continuum to be amplified was selected with an interference filter and the gain dye was selected to match this wavelength region. Energies of 100-200 μJ per pulse were obtained in the near infrared (IR) region. Later, the Bell Labs researchers generated 60-fs, 0.5-μJ, near IR pulses at 8 kHz [Becker *et. al.* (1988,1989)]. They selected the IR portion of the continuum to be amplified with a prism filter which also precompensated for the chirp induced by the amplifier. They used a standard CVL-pumped bow-tie amplifier which consisted mainly of reflective optical components to avoid chromatic aberrations and GVD. A 5-μm-thick GaAs multiple quantum well was used as the saturable absorber resulting in less than a percent of ASE.

In the bow-tie amplifier configuration, each gain pass must be aligned separately, and each pass does not coincide with the same spot on the gain jet. Thus each pass cannot traverse the region of maximum gain produced by the focused CVL beam unless the CVL is focused to a large spot size. A large CVL spot size reduces the population inversion in the gain dye and thus the potential gain. In addition, each pass cannot be focused on the gain jet without using many lenses. Lenses increase the undesirable GVD. In a two-mirror telescopic amplifier [Khoroshilov *et. al.* (1988)], as illustrated in Figure 2.7, the confocal geometry of the resonator inherently focuses each beam at the common focus of the two mirrors resulting in higher efficiency amplification when the CVL is focused on the common

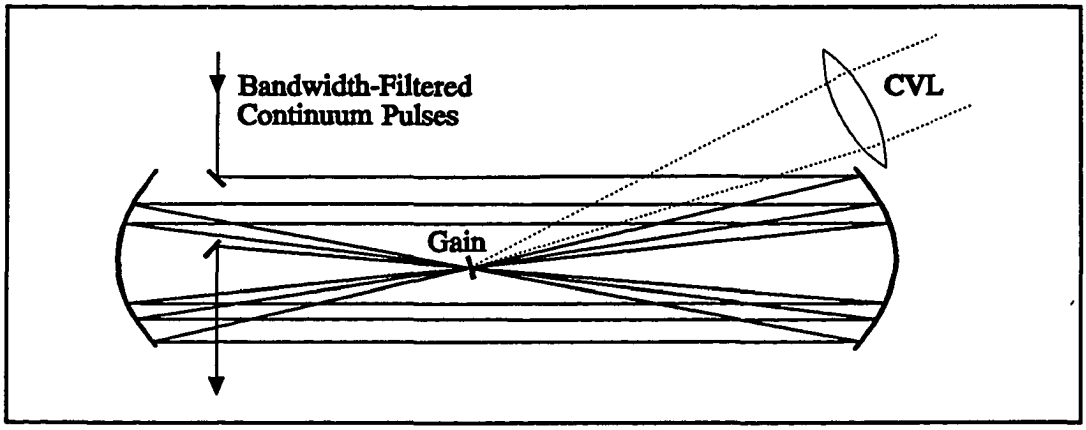

Figure 2.7 Tunable-pump telescopic amplifier

spot. Since no lenses are required, only the gain dye introduces GVD. In addition, when the two mirrors are correctly aligned, proper adjustment of the initial pass automatically aligns the subsequent passes. We use this two-mirror telescopic amplifying scheme to obtain tunable pump pulses. The focal lengths of the two mirrors (12 and 15 cm) are different to allow beam walk-off. The gain medium (LDS 751 in EG) dye jet is located at the common focus of the two mirrors and is pumped with approximately 15 W of a second CVL at 8.5 kHz. The second CVL is also triggered by the CPM and then optically delayed to synchronize the CVL pulse and bandwidth-filtered continuum pulse at the gain jet. It was necessary to block the center of one mirror to prevent lasing. The 760-nm, 10-nm BW portion of the continuum, which was selected with a tilted 780-nm interference filter, is passed through the gain dye six times resulting in a gain of $\approx 5 \times 10^4$. The resulting pulses are compressed with another prism assembly yielding $\approx$1-μJ, 130-fs pump pulses.

Transient Pump-Probe Spectroscopy

To perform transient pump-probe spectroscopy, the pump beam and continuum probe beam are focused and overlapped temporally and spectrally on the sample as illustrated

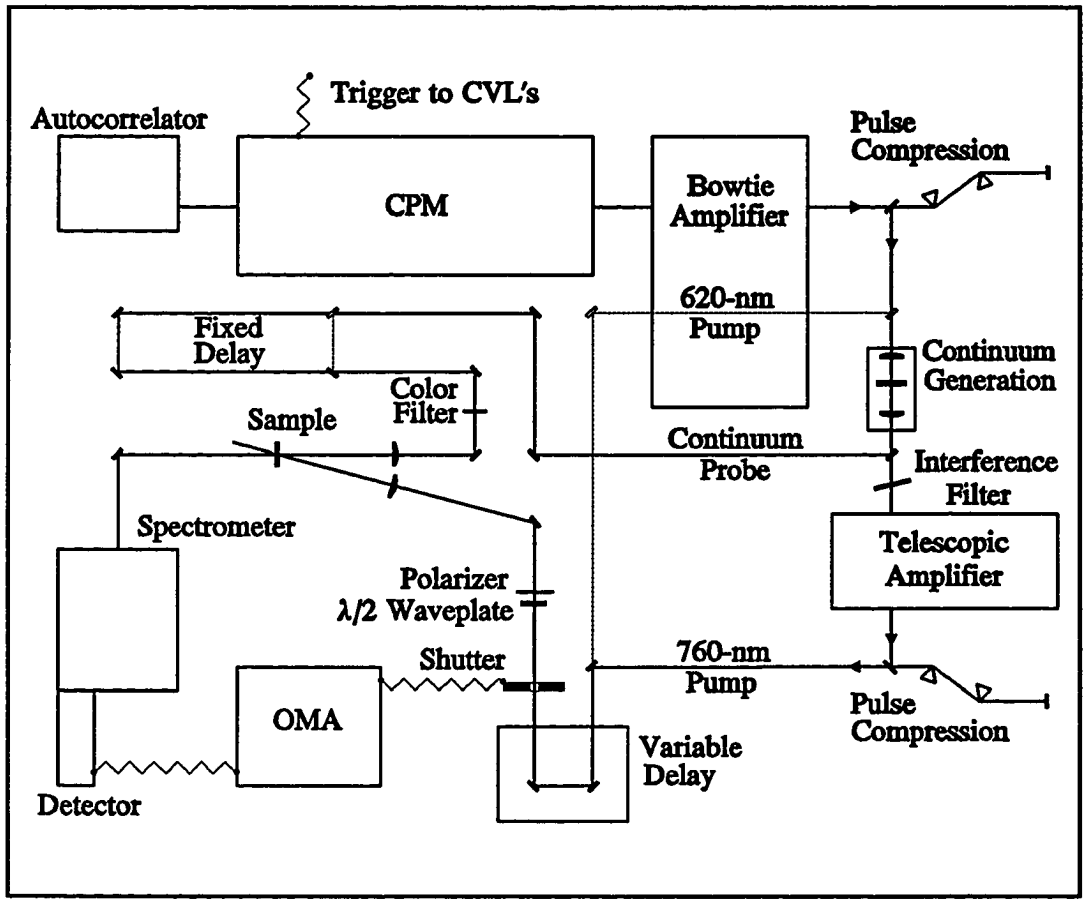

Figure 2.8 Schematic of femtosecond facility

in Figure 2.8. The beams are separated by ≈15°. For the case of the 760-nm pump, where the pump pulse traverses ≈1.5 m through the second amplifier, a sizeable optical delay path is required for the probe beam such that the pump and probe pulses arrive at the sample simultaneously. The time delay of the pump beam is varied with a Klinger-stepper-motor-controlled delay arm. Negative time delays indicate that the probe pulse precedes the pump pulse; positive times, that the probe pulse succeeds the pump pulse. The probe beam is sent through a color filter to control its spectral shape, and the pump beam is sent through a half-wave retardation plate and a polarizer to control its polarization state. The pump beam is

also sent through a shutter to block the pump during data acquisition. Both beams are focused with separate lenses to ≈30-μm diameter spots on the sample. To locate the overlap of the two pulses, a lithium iodate ($LiIO_3$) second-harmonic crystal is placed at the sample location. As with the autocorrelator, at the bisecting angle of the two beams a phase-matching condition of the crystal is met when the pulses are temporally and spatially overlapped. This background-free sum-frequency signal is monitored with a PMT. This signal is located and maximized temporally by scanning the stepper motor, and thus the time delay of the pump pulse. The signal is then maximized spatially by adjusting the positions of the spots with the separate lenses. When the overlap is optimized, the crystal is removed and the sample is replaced.

Differential transmission (DT) spectra

After passing through the sample, the probe beam is focused onto the 50-μm slit of a 0.34-m focal length spectrometer with a 300 line/mm blazed grating. The diffracted light is incident on a 25-mm, 1024-element, linear diode-array detector which is connected to an EG&G optical multichannel analyzer (OMA) III. The OMA then monitors the light intensity of the probe beam over a 120-nm BW with a resolution of a few angstroms. The intensity of the probe beam varies by orders of magnitude over the continuum BW, being most intense around 620 nm, the generation frequency. Different color filters are placed in the probe arm for the different spectral regions to maximize the spectral content of the pulse in the desired region and to prevent damage to the detector.

To monitor the pump-induced transmission changes to a sample as a function of time, the differential transmission (DT) spectra of the sample is measured at various time delays between the pump and probe beams. The $DT = (T-T_0)/T_0$ where T and T_0 are the pump-modified and linear transmission, respectively. DT spectra are more sensitive to small

changes than absolute transmission spectra. For the selected time delay, as dictated by the position of the stepper motor, the OMA scans (16 msec/scan) the transmitted probe intensity with the pump shutter open and then again with the pump shutter closed to obtain I_T and I_{T0}, respectively. The shutter is triggered by the OMA and the scans are saved in separate OMA registers. As many as 1000 to 5000 consecutive scans are performed, depending on the desired experimental accuracy, and the results are added alternately to the two data registers. Recalling that $T = I_T/I_0$ and $T_0 = I_{T0}/I_0$ where I_0 is probe intensity entering the sample, we find that $DT = (I_T - I_{T0})/I_{T0}$. Using a keystroke program in the OMA, the experiment is executed, the background subtracted from each register, and the DT spectrum computed for the selected time delay. The process is repeated at other time delays to follow the evolution of the pump-induced transmission changes.

The remaining GVD in the probe pulse induces a small amount of near linear chirp in the near IR spectral region of the probe pulse. This chirp is measured by sending the sum-frequency signal generated by a second harmonic crystal at the sample location into the OMA. Using the YT mode of the OMA, the relative time delays between different wavelength regions are measured as the time delay between the pulses is continuously varied with the stepper motor. The resulting "chirp" profile is fit to a parabola. The DT spectra are then corrected subsequent to data acquisition using a "dechirping" program written in the BASIC language (Appendix A) which requests the chirp parabola coefficients. Because of the chirp in the probe pulse, the precise location of "zero" time, when the pump and probe pulses are temporally overlapped, is accurate to ±100 fs. "Zero" time can often be inferred with greater accuracy by examining the evolution of the DT spectral curves.

When DT curves are required over a BW larger than 120 nm, the experiment must be repeated for adjacent but overlapping spectral regions. For each separate spectral region, the

color filter in the probe arm must be changed and the temporal overlap of the pulses readjusted. In addition, the chirp in the pulse is different for separate spectral regions. The time delays of DT curves obtained for adjacent spectral regions are therefore not consistent. Significant spectral overlap between adjacent curves allows the time delays of the curves to be matched up by comparing the relative magnitudes of the DT signals from adjacent regions.

Fast data acquisition system

It is often desirable to look at the transmission changes of a sample continuously in time at discrete wavelengths (decay curves) as opposed to continuously in wavelength at discrete times (DT spectra). The fast data acquisition (FDA) system was designed for this purpose. Here, the probe beam is split before the sample; one part is overlapped with the pump beam, the other travels through an unpumped portion of the sample. The desired wavelength region of the resulting I_T and I_{T0} beams are selected using a monochromator and simultaneously monitored using two PMT's. The PMT signals are sent to a fast analog to digital converter, a Crate PC controller, and then into a 16-MHz personal computer. The DT is computed for every pulse at the 8.5-kHz repetition rate. In addition, FDA discriminates every laser pulse and computes the DTS only for those pulses within the selected intensity window. For typical decay curves, the DT for 17,000 laser pulses are averaged for each time increment, and the stepper motor is then advanced to the next position. The experiment is operated by a program written in the C language using the personal computer.

Using this femtosecond facility, the ultrafast excitation and decay dynamics of many physical systems can be studied. This manuscript concentrates on the ultrafast dynamics of organic systems, namely aluminum phthalocyanine thin films and composite dye-doped PMMA thin films and etalons.

CHAPTER 3

PROPERTIES OF PHTHALOCYANINE MOLECULES AND ALUMINUM PHTHALOCYANINE THIN FILMS

The metallophthalocyanine (MPc) family of organic molecules has received much attention from the optical community because they exhibit 10^{-11}-10^{-9} esu third order optical nonlinearities and picosecond excitonic lifetimes, as well as interesting photoconductivity properties. MPcs are synthetic in origin but structurally similar to the much studied and biologically important porphyrins, as well as chlorophyll, hemoglobin and vitamin B_{12}. MPc molecules consist of a metal (M) ion centered in a planar aromatic phthalocyanine (Pc) ring. Figure 3.1 shows the molecular structure of fluoro-aluminum phthalocyanine (FAlPc) where aluminum is the central metal. *Phthalocyanine* comes from the Greek na*phtha* (rockoil) and *cyanide* (dark blue). Since the systematic categorization of MPcs in the 1930's, they have been intrinsically used as commercial pigments and dyes. In addition, MPcs are thermally stable up to 400° C, chemically stable, and have a high laser damage threshold. H_2Pc has been used as the saturable absorber in a passively Q-switched ruby laser [Kosonocky *et. al.* (1965)]. Thin films of MPcs can be easily vapor sublimed with exceptional purity for organic systems (10^{14}-10^{15} traps/cm^3) [Simon and André (1985)]. MPc films are interesting organic materials for use in photocopy, laser printer, photovoltaic solar cell, photoconductive, and photoelectrochemical applications [Klofta *et. al.* (1985), Rieke (1984)]. Since the absorption [Laurs and Heiland (1987)] and resistivity [Barger *et. al.* (1985)] of MPc films change upon

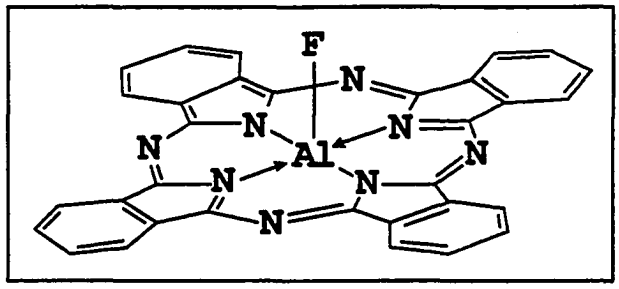

Figure 3.1 Molecular structure of FAlPc

exposure to various gases, they may be effective as chemical sensors. MPcs are also useful for optical data storage. CuPc has been used for erasable optical memory [Kobayashi *et. al.* (1988)], and H_2Pc, TePc, and CuPc, for optical recording [Dautartas *et. al.* (1985), Goto *et. al.* (1984)].

Phthalocyanine Molecules

The planar aromatic Pc ring contains a two-dimensional conjugated π-electron system where 18 π-electrons are distributed over the 16 sites of the inner ring. This delocalized system has two highly allowed π-π^* electronic transitions resulting in two intense optical absorption bands: the Q band at 600-800 nm and the B or Soret band at 300-400 nm. These two bands, both of E_u symmetry, are attributed to the $a_{1u}(\pi)$ to $e_g(\pi^*)$ and the $a_{2u}(\pi)$ to $e_g(\pi^*)$ transitions, respectively, and have absorption coefficients $\alpha \approx 2 \times 10^5$ cm^{-1}. The metal ion located in the center of the Pc ligand has little effect on the absorption bands, thus the bands are attributed to the delocalized π-electrons of the Pc ring. Replacing the metal ion with H_2, however, lifts the degeneracy and splits the bands.

MPcs provide a very versatile chemical system as more than 70 MPcs are known [Simon and André (1985)]. In this manuscript we study the ultrafast optical nonlinear properties of FAlPc and chloro-aluminum phthalocyanine (ClAlPc). The FAlPc molecule consists of an aluminum ion centered in the phthalocyanine ring with a fluorine ion bonded to the aluminum ion out of the plane of the Pc ring as illustrated in Figure 3.1. Similarly, in the ClAlPc molecule, a chlorine ion is bonded to the aluminum. The Q-band absorbance spectrum of the FAlPc monomer (FAlPc dissolved in pyridine solution) is shown (in arbitrary units) by the dashed line in Figure 3.2. The smaller peaks at higher energy are vibronic sidebands. A vibronic transition involves the π-π^* optical transition and an excited-state vibrational mode of the molecule.

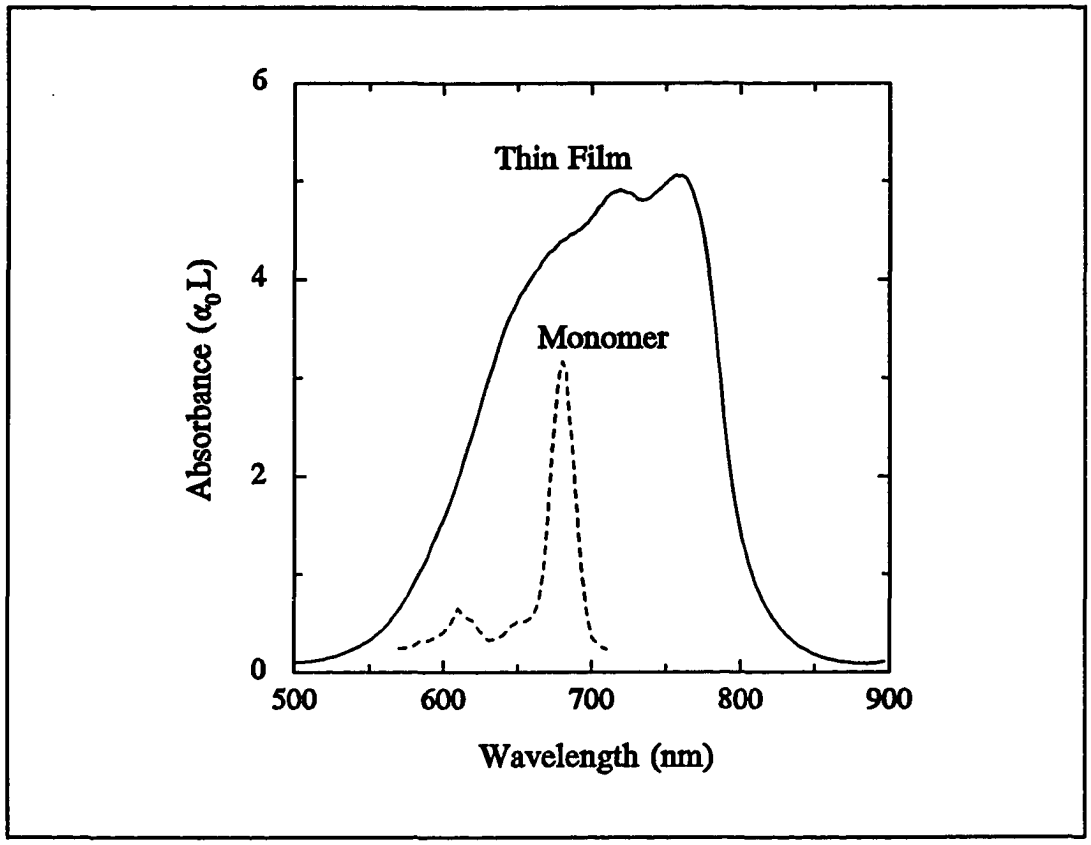

Figure 3.2 Absorbance spectra of FAlPc monomer and thin film

Aluminum Phthalocyanine (AlPc) Thin Films

When these MPc molecules are sublimed into solid thin films, the absorption bands become broader than for the monomer due to intermolecular interactions. FAlPc sublimed films are composed of microcrystallites which can be interspersed with amorphous material. These microcrystallites can consist of linear, cofacial, "polymeric" stacks of AlPc-F, with the adjacent Pcs aligned along the $Al^{\delta+}$-$F^{\delta-}\cdots Al^{\delta+}$-$F^{\delta-}\cdots$ axis [Linsky *et. al.* (1980)]. Other crystallites are possible, where the adjacent Pc rings are held merely by van der Waals forces. The van der Waals dimensions of the Pc ring are ≈13 Å in diameter [Dann *et. al.* (1990)] and ≈3.3 Å in height [Linsky *et. al.* (1980]. For the Al-F bond, the van der Waals diameters are

$1.07_{Al}+2.57_{F}=3.64$ $Å_{Al-F}$. The π-electron orbitals of FAlPc are thought to have a height of $\approx$4 Å [Armstrong (1990]. Thus, when FAlPc molecules are packed at near van der Waals distances, the π-electron orbitals of vertically adjacent FAlPc molecules overlap, broadening the linear spectrum and splitting the normally degenerate excited-state transitions.

The molecular exciton model [Kasha (1976), Sauer *et. al.* (1990)] shows how the splitting depends on the orientation of adjacent molecules (in our case, the Pc rings) and their transition dipole moments. This model was originally developed for naphthalene and anthracene and has not been rigorously extrapolated to phthalocyanines. It is clear, however, that when molecules are placed at van der Waals distances, splitting of the excited-state transitions occur. When adjacent molecules have parallel transition dipole moments (θ=0°), the higher energy transition dominates, and a blue-shift of the linear absorption is induced. The linear spectrum is red-shifted when transition dipole moments of adjacent molecules are oriented end-to-end (θ=180°). This "Davydov splitting" is illustrated in Figure 3.3. The dashed lines indicate vibrational levels. For the parallel case, when two transition dipole moments are in-phase, the electrostatic repulsion between them increases the dipole transition energy. When the dipole moments are out-of-phase, the transition energy is reduced by the electrostatic attraction. Since both molecules will be influenced simultaneously by an incident electric field, the dipole moments can only be excited in-phase, and thus only the blue-shifted transition is allowed. Analogously, for the end-to-end case, the excitable in-phase components are electrostatically attractive leading to a reduction in the allowed transition energy. When intermediate angles or oblique orientations occur between adjacent molecules, both red- and blue-shifts of the excited state can be dipole allowed.

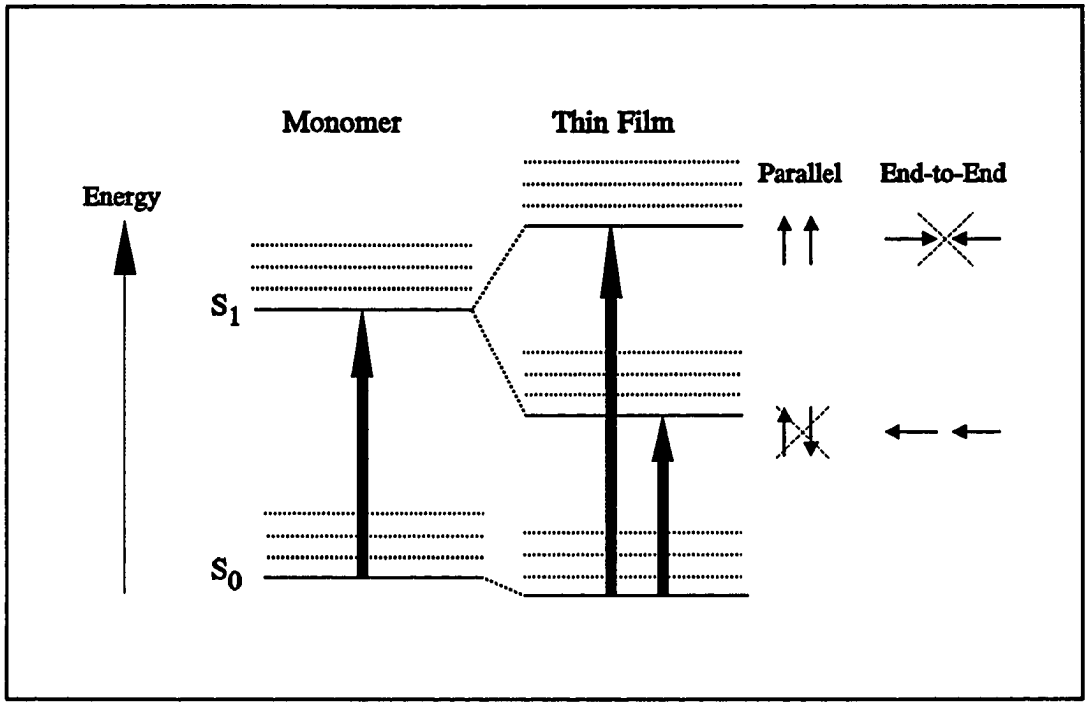

Figure 3.3 Davydov Splitting

The ≈0.2-μm thick FAlPc polycrystalline thin film studied here was vapor deposited onto a silica substrate held at ca. 100° C and 10^{-8} torr, at a rate of ca. 25 Å/min. (The ClAlPc thin film was sublimed under similar conditions.) The Q-band absorbance spectrum of the FAlPc thin film, shown by the solid line in Figure 3.2, is broadened, with considerable red-shifting and some blue-shifting relative to the spectral response of the monomer. This suggests the presence of at least two distinct phases of the Pc. Collinear, cofacially-stacked phases have been identified for Pcs such as AlPc-F [Linsky *et. al.* (1980)], which induce a blue-shift of the thin film absorption peak relative to the monomer [Sims *et. al.* (1989), Hoshi *et. al.* (1990), Sauer *et. al.* (1990), Marks (1985)]. A staggered, slipped-stack phase has also been identified which induces a red-shift and possible splitting of the Q-band [Sims *et. al.* (1989)]. The blue-shifted, cofacially-stacked phases are associated with prismatic/block-

type crystallite formations observed in electron micrographs, while the red-shifted, slipped-stack phases appear related to a platelet crystallite morphology [Sims *et. al.* (1989)]. For the deposition conditions used to create the FAlPc films discussed here, it is likely that both forms are present along with a small percentage of amorphous material. X-ray diffraction measurements of our sublimed FAlPc thin film yield one strong reflection at 2θ=27.0°, consistent with Pc ring spacings of ≈3.3 Å, and additional unresolved reflection peaks corresponding to less ordered phases. The polycrystalline nature of our thin film, and the consequent distribution of dipole interactions at different molecular sites, results in an inhomogeneous broadening of the Q-band transition.

The red-shifted phases of the Q-band in our FAlPc thin film were pumped with 760-nm, 130-fs pump pulses and the transmission changes studied using transient pump-probe spectroscopy. Polarization-dependent spectral hole burning was observed.

CHAPTER 4

POLARIZATION-DEPENDENT SPECTRAL HOLE BURNING IN A FLUORO-ALUMINUM PHTHALOCYANINE THIN FILM

Ultrafast decay of the optical nonlinearities is a fundamental requirement for successful application of phthalocyanine materials to the next generation of high-speed optoelectronic devices. Ultrafast phenomena, such as coherent transients and nonequilibrium spectral hole burning, have been observed in both inorganic semiconductors and organic solutions using transient pump-probe spectroscopy. Spectral holes induced by nonthermal carrier populations [Oudar *et. al.* (1985), Knox *et. al.* (1986,1988), Lin *et. al.* (1988)] and coherent oscillations attributed to coupling between the light field and the material [Fluegel *et. al.* (1987), Lindberg and Koch (1988a,b), Joffre *et. al.* (1988), Sokoloff *et. al.* (1988)] have been examined in many inorganic semiconductors.

In organic dye solutions, both coherent coupling [Heinz *et. al.* (1984), Palfrey and Heinz (1985)] and population [Brito Cruz *et. al.* (1986), Shank *et. al.* (1986)] effects have been studied. The spectral hole burning in dyes was first attributed to nonequilibrium exciton populations [Brito Cruz *et. al.* (1986)], and later to coherent pump-probe coupling [Pollard *et. al.* (1989)]. In addition, coherent spectral holes were observed and modeled theoretically in Bacteriorhodopsin suspensions [Mathies *et. al.* (1988a,b), Pollard *et. al.* (1989)]. While the hole burning processes in organic solutions have been treated theoretically [Loring *et. al.* (1987), Brito Cruz *et. al.* (1988), Vogel *et. al.* (1988), Mathies *et. al.* (1988a), Pollard *et. al.* (1989)], the interpretation of the relaxation mechanisms is complicated by the fact that vibronic coupling of the solvent molecules may alter the electronic properties of the dye molecules being studied. In ultrafast pump-probe experiments on solid-phase phthalocyanine thin films, exciton-exciton annihilation [Greene and Millard (1985a,b),

Millard and Greene (1985), Ho and Peyghambarian (1988)] and exciton-phonon coupling (internal conversion) [Ho and Peyghambarian (1988)] were identified as prominent relaxation mechanisms. In these studies, however, the pump pulses were located at the high energy edge of the absorption band, and spectral holes were not observed.

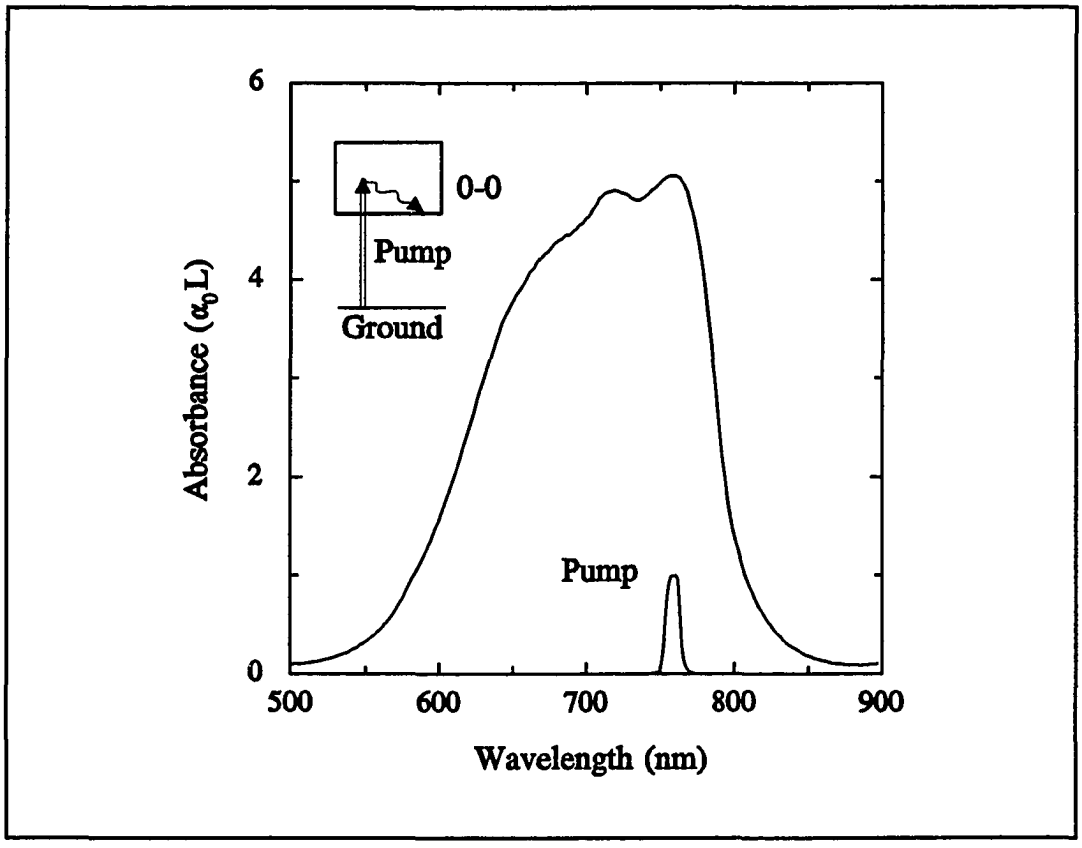

Figure 4.1 Spectral position of pump pulse in Q-band

We pumped a solid-phase organic semiconductor, our FAlPc sublimed polycrystalline thin film, directly into the Q-band absorption peak with 3.9-GW/cm^2, 130-fs, 760-nm pulses at room-temperature as indicated in Figure 4.1. The magnitude of the pump is shown in arbitrary units. We observe a polarization-dependent spectral hole coincident with the pump pulse which is seen only when the probe pulse is polarized parallel to the pump pulse

[Williams *et. al.* (1991a,b)]. This type of polarization-dependent spectral hole burning has not been observed in inorganic semiconductors.

Ultrafast Polarization-Dependent Spectral Hole

The resulting DT spectral curves obtained with the pump and probe pulses both s-polarized clearly illustrate the evolution of a spectral hole burned by the 760-nm pump pulse [Figure 4.2(a)]. Negative times indicate that the probe pulse precedes the pump pulse; positive times, that the probe pulse succeeds the pump pulse. The hole is observed as a peak in the DT curves, spectrally coincident with the pump pulse at early times. The hole broadens in time, and at 40 fs the coincident spectral hole is broader than the pump. In addition, a shoulder develops on the low energy side of the burned hole. In the 200-fs spectrum of Figure 4.2(b), the spectral hole has completely disappeared and the shoulder has evolved into a broad peak at the bottom of the absorption band. The linear absorbance is shown with a dashed line for reference. In contrast, when the pump and probe pulses are orthogonally polarized [Fig. 4.3(a)], the spectral hole is not detected and only the growth of the broad peak at the bottom of the absorption band is observed in the DT spectra. At later times, the broad bleaching signal at the bottom of the band decays with increasing time delay for both probe polarization directions as shown in Figures 4.2(b) and 4.3(b).

Coherent Coupling and Nonequilibrium Exciton Population

The probe-polarization dependence of the spectral hole in the early-time DT spectra can be explained as follows. Since the spectral hole is observed only when the pump and probe pulses are temporally overlapped, we surmise that the spectral hole is predominantly a coherent phenomenon. That is, the pump pulse perturbs and coherently drives the components of the π-π^* excitonic transition dipole moments which are parallel to the electric

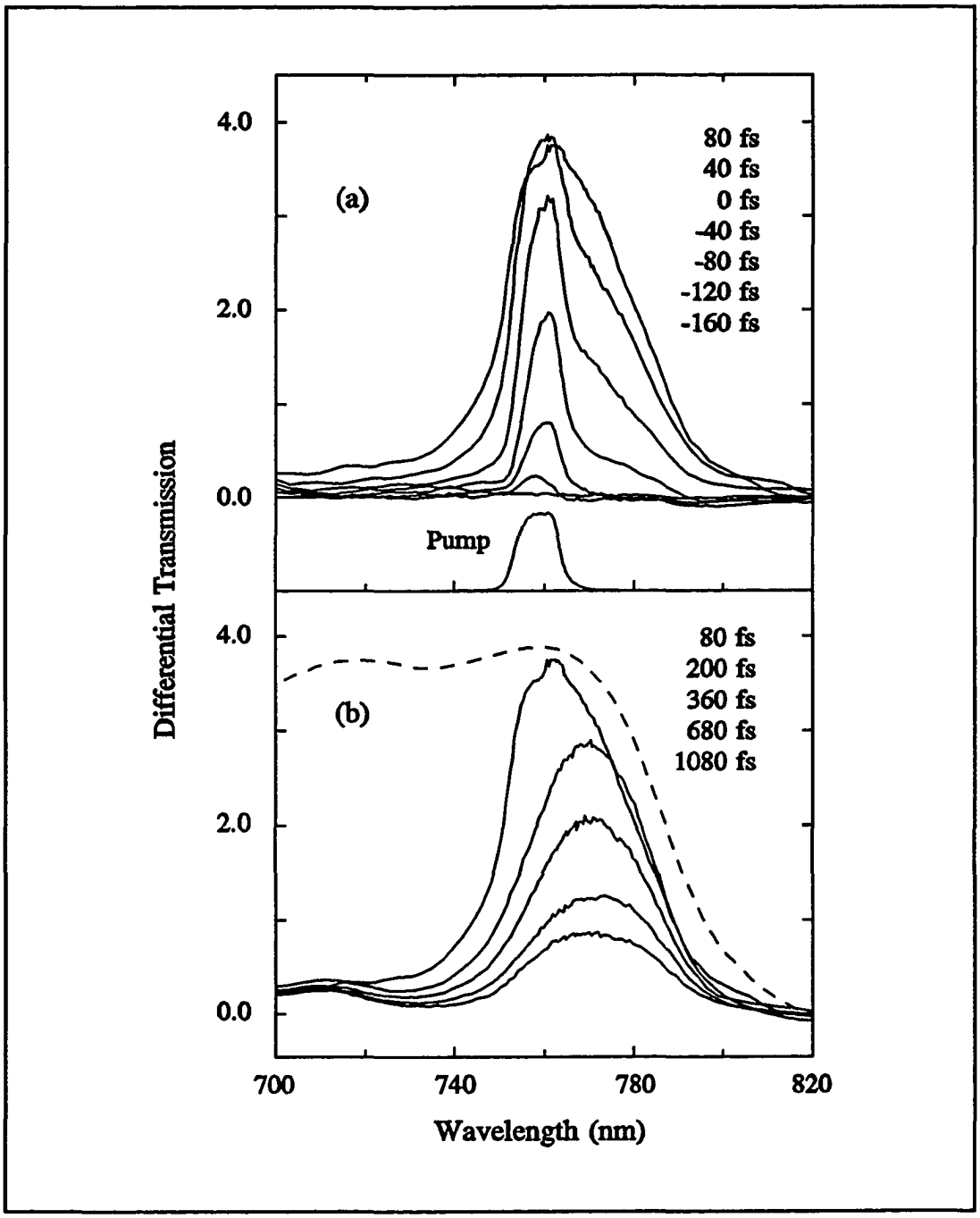

Figure 4.2 DT spectra with pump and probe pulses polarized parallel

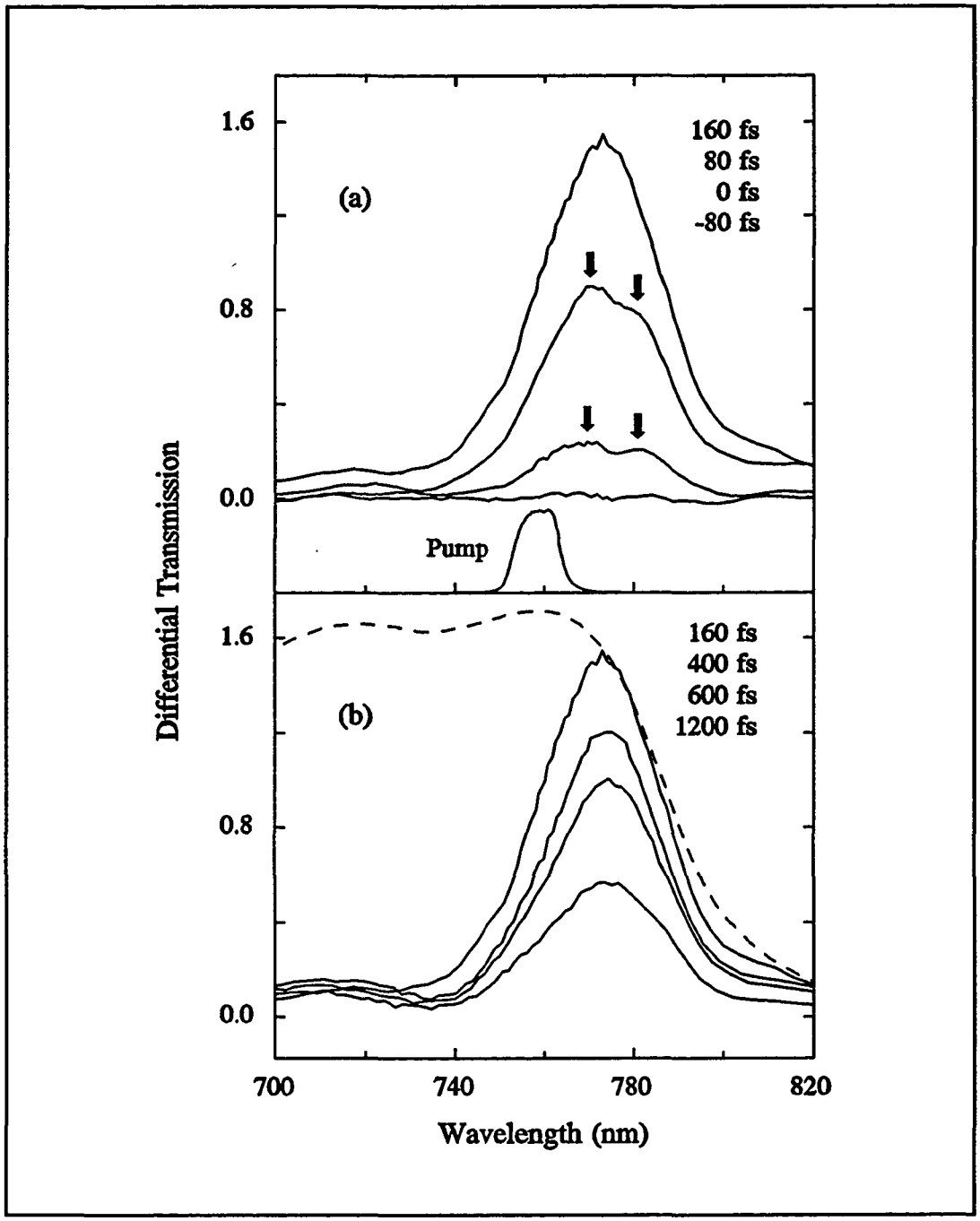

Figure 4.3 DT spectra with pump and probe pulses orthogonally polarized

field of the pump. A parallel probe field interacts with the pump-induced polarization density while a perpendicular probe field does not. Thus a coherent spectral hole is observed at the pump position only when the pump and probe pulses are polarized parallel and temporally overlapped. This implies that orthogonal polarization states of the molecule, which lie in the plane of the phthalocyanine ring, are effectively uncoupled.

The early evolution of the spectral hole resembles similar effects observed in inorganic semiconductors where population spectral holes evolve from coherent oscillations with increasing temporal overlap [Fluegel *et. al.* (1987), Joffre *et. al.* (1988), Sokoloff *et. al.* (1988)]. In our case, however, oscillations are not observed, except for a small oscillation in the -160-fs curve. This behavior agrees with theory [Fluegel *et. al.* (1987), Lindberg and Koch (1988b), Sokoloff *et. al.* (1988)] which predicts that a very rapid intraband population decay decreases the amplitude of the oscillations relative to the central peak such that only the central peak is observed.

In addition, because the observed central peak becomes spectrally broader than the pump pulse, the spectral hole presumably also has a rapidly-decaying real exciton population component. Rapid scattering out of the coherently-driven states results in a nonequilibrium excitonic population at the pump location. This "polarized" population, which does not interact with an orthogonal probe but bleaches (blocks) the occupied transitions for a parallel probe, then depolarizes and relaxes to the bottom of the π-π^* excited-state manifold. At later times, the broad peak observed at lower energies for both probe polarizations is attributed to bleaching of the transitions at the bottom of Q-band by the "depolarized" exciton population as discussed below.

Exciton Relaxation within the Q Band

It is important to note that we are creating an exciton population in the wavelength region where the phases of the FAlPc thin film absorb light that is far to the red of that absorbed by the isolated monomer or a linear, cofacial AlPc-F stack. The bottom of the red-shifted 0-0 manifold is located spectrally below the pump as illustrated in the inset of Figure 4.1. (A 0-0 transition indicates a purely electronic, S_0-S_1, transition with no vibrational contribution. A 0-1 transition indicates a transition from S_0 to a first vibrational level of the S_1 state.) In the -40-fs spectrum of Figure 4.2(a), the occupation of the 0-0 states at the bottom of the manifold is first observed. This occurs within 120 fs after the onset of the hole burned by the leading edge of the pump pulse, again indicating a rapid exciton population decay. The transmission of both the parallel and perpendicular probes increase due to bleaching of the 0-0 transitions at the bottom of the π-π^* singlet manifold by the scattered, depolarized exciton population. We attribute the difference in the DT magnitudes at the bottom of the Q band between the parallel and perpendicular cases to incomplete depolarization of the nonequilibrium exciton population at early times.

Two spectrally-separated bumps (indicated by arrows) are observed in the 0 fs and 80 fs DT spectra of Figure 4.3(a) for the perpendicularly-polarized case. The $\approx$220 cm^{-1} peak-to-peak separation of these components corresponds well to the metal-nitrogen in-plane stretching vibration of metallophthalocyanine molecules [Aroca *et. al.* (1989); Aroca *et. al.* (1990)]. This suggests that the 0-0 transitions may be accompanied by vibronic 0-1 transitions. As the exciton population evolves, the 0-0 and 0-1 states of many different molecules become occupied resulting in a single broad DT spectral feature centered at about 775 nm. In the parallel pump-probe case, it is probable that the population of the 0-1 transitions is masked by the spectral hole.

Decoupled Orthogonal Polarization States

Rotating the thin film in the plane perpendicular to the incident pump beam does not alter the results presented above. Our results differ from fs spectroscopic results on GaAs where a spectral hole is observed regardless of the probe polarization [Lin *et. al.*(1988)]. In such inorganic semiconductors, the orthogonal polarization states are effectively coupled. The orthogonal polarization states in Pc molecules appear to be decoupled, presumably due to local deformations of the conjugated π-electron systems.

Exciton Relaxation into Ground and Triplet States

These ultrafast results demonstrate that the exciton population rapidly depolarizes and relaxes to the bottom of the excited-state manifold within 200 fs. This relaxation is followed by the decay of the excited molecules back to the ground state and into triplet states. Exciton-exciton and exciton-phonon scattering contribute to this subsequent decay. This decay is observed in Figs. 4.2(b) and 4.3(b) where the DT signals decrease with increasing time. The exciton relaxation dynamics involving the triplet and ground states in AlPc thin films are presented in detail in Chapter 6 after a brief review of dynamics in Pc solutions and thin films in Chapter 5.

CHAPTER 5

RELAXATION DYNAMICS IN PHTHALOCYANINE SOLUTIONS AND THIN FILMS

The relaxation dynamics of excited molecules in solution [Robinson and Frosch (1963), Byrne *et. al.* (1965), Kobayashi and Nagakura (1972a), Kenney-Wallace (1984)] and crystalline solids [Bergman *et. al.* (1967), Suna (1970), Kobayashi and Nagakura (1972b), Powell and Soos (1975), Trout *et. al.* (1984)] have been studied extensively. Molecular systems generally consist of a ground state, S_0, a first excited singlet state, S_1, and a triplet

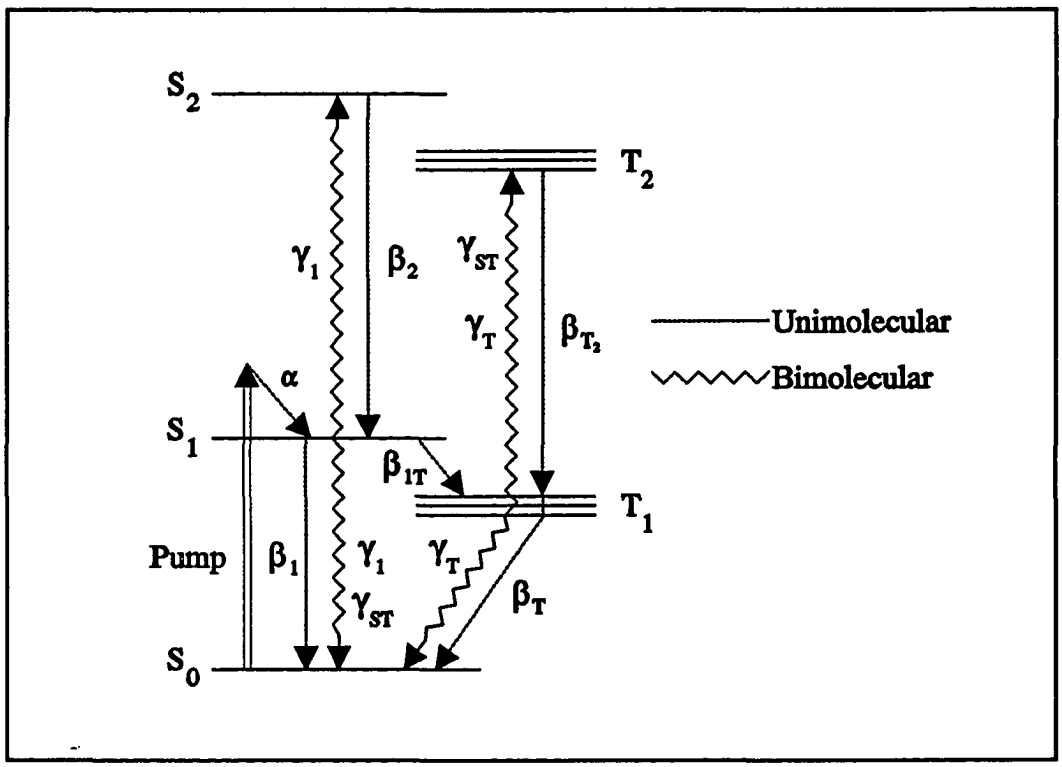

Figure 5.1 Molecular energy levels

state manifold, T_1 as pictured in Figure 5.1. Singlet-triplet transitions are formally forbidden as they have different spin multiplicity. When molecules are excited, they can

decay back to the ground state either radiatively yielding luminescence or nonradiatively inducing vibrations and eventually heat. Radiative decay from S_1 to S_0 is called fluorescence; from T_1 to S_0, phosphorescence. Nonradiative decay occurs through the interaction of vibrational modes or through bimolecular collisions. Nonradiative vibrational decay between singlet states is called internal conversion; nonradiative vibrational decay between singlet states and triplet or other spin-forbidden electronic states is called intersystem crossing.

MPc Solution Dynamics

The dynamics of MPcs in solution have been studied extensively [Vincett *et. al.* (1970), Huang *et. al.* (1977), Brannon and Magde (1980), Simon and André (1985), Millard and Greene (1985)]. Since molecular vibrational decay within a given excited state (dephasing) occurs on a few picosecond time scale in solutions, most photoreactions occur from the lowest vibrational level of the excited state [Simon and André (1985)]. Fluorescence lifetimes for most MPcs are on the order of a few nanoseconds [Simon and André (1985), Brannon and Magde (1980)]. In fact, the natural radiative lifetime of MPcs (about 10 ns) varies little with the metal cation [Simon and André (1985), Millard and Greene (1985), Brannon and Magde (1980)].

Nonradiative decays from the first excited singlet state (Q band) occur on a picosecond time scale for MPcs in solution [Millard and Greene (1985), Simon and André (1985)]. S_1 to S_0 internal conversion transitions are inefficient for rigid, planar, π-electron systems as well as for molecules which possess a center of symmetry [Simon and André (1985), Brannon and Magde (1980)] as is the case for MPcs. In addition, S_1 to S_0 internal conversion is slow in MPcs because the energy gap (about 15,000 cm^{-1}) is much larger than vibrational energies (600-1400 cm^{-1} for skeletal stretch and bending vibrations [Byrne *et. al.* (1965)], 550 cm^{-1} for the Al-F vibration in FAlPc [Linsky *et. al.* (1980)], 0 to several

hundred cm^{-1} for lattice phonons). S_1 to T_1 intersystem crossing, which is fast because of the smaller energy gap (about 5000 cm^{-1}), is expected to be the dominant decay pathway from the first excited singlet state, especially for those Pcs which exhibit appreciable spin-orbit coupling [Kosonocky *et. al.* (1965), Menzel *et. al.* (1972), Huang *et. al.* (1977)]. Spin-orbit coupling increases with the size of the central metal ion and with the number of d-orbital electrons in the metal. S_1 to T_1 intersystem crossing in MPc solutions becomes more enhanced as the central metal ions become heavier [Menzel *et. al.* (1972), Huang *et. al.* (1977)]. Since most nonradiative decay from S_1 occurs over the small S_1 to T_1 energy gap, little thermal degradation of the first excited singlet of MPcs in solution is expected [Simon and André (1985)].

Triplet states, on the other hand, decay mostly though nonradiative vibrational decay to the ground state inducing heat. Phosphorescence quantum yields are generally very low with lifetimes varying from microseconds for heavy metal cations to as long as milliseconds for light metal cations [Huang *et. al.* (1977), Simon and André (1985)]. Nonradiative vibrational decays from the triplet levels to the ground state occur slowly, on a microsecond time scale [Simon and André (1985)] again because the energy gap (about 10,000 cm^{-1}) is large relative to vibrational energies and because the transition is spin-forbidden.

Molecular Solid Dynamics

In the molecular solid, a quasicontinuum of "external" crystal lattice modes is supported in addition to the "internal" molecular vibrations. The molecular vibrational modes easily relax into other internal modes plus "external" crystal lattice modes thus enhancing nonradiative decay [Trout *et. al.* (1984)]. The electronic energy transformed into lattice vibrations is then converted into heat.

At low exciton densities, decay lifetimes are determined by unimolecular exponential decay processes such as radiative luminescence and nonradiative vibrational relaxation (exciton-phonon coupling). (If vibrational relaxation leads to a rise in the lattice temperature, exponential decay would not be expected [Greene *et. al.* (1987)].) When large exciton densities are present, bimolecular exciton-exciton annihilation (fusion or quenching) becomes important and decays are no longer exponential. Exciton-exciton annihilation is a nonradiative scattering process consisting of two rate determining steps: exciton motion (migration) and exciton-exciton collision resulting in destruction (ionization) of one exciton and further excitation of the other [Suna (1970)]. As such, exciton annihilation is exciton-density (or excitation-intensity) dependent. Exciton migration in molecular crystals at room temperature is often described as a random walk process where excitons hop incoherently through the molecular lattice. Exciton-phonon interaction contributes to the hopping of the excitons [Kobayashi and Nagadura (1972b)]. When a pair of singlet excitons collide, one exciton may be excited to a higher level energy state (or converted to a free electron) using the energy produced by the ionization of the other exciton when its associated molecule returns nonradiatively to the ground state:

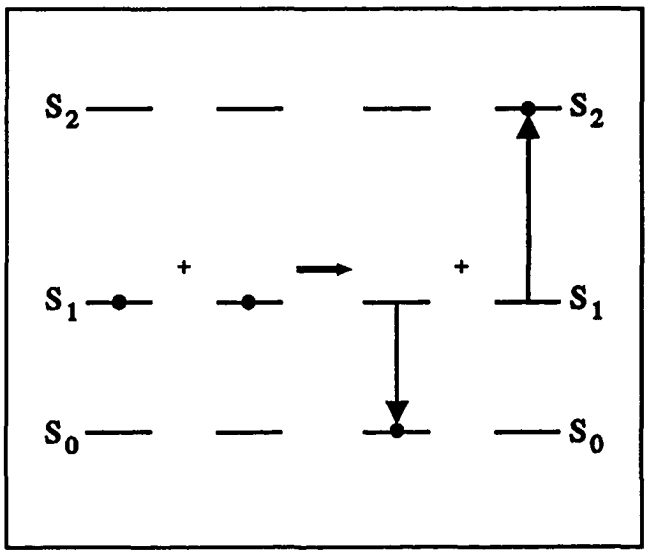

Figure 5.2 Bimolecular annihilation

$$S_1 + S_1 \xrightarrow{\gamma_1} S_0 + S_2.$$

Bimolecular exciton-exciton annihilation is illustrated schematically in Figure 5.2. This compares to the Auger autoionization process which is similarly important for high exciton densities in inorganic semiconductor crystals [Sermage *et. al.* (1985)]. Singlet-triplet annihilation (or fusion), where

$$S_1 + T_1 \xrightarrow{\gamma_{ST}} S_0 + T_2,$$

has been observed during fluorescence quenching experiments on H_2Pc solutions [Menzel and Sharp (1977)]. Bimolecular processes in solutions [Kobayashi and Nagakura (1972a)] and in molecular solids depend on dipole-dipole interactions between transition moments. The annihilation probability is proportional to R^{-6}, where R is the distance between excitons [Kobayashi and Nagakura (1972b)]. In general, exciton-exciton annihilation is assumed to occur between excitons on adjacent lattice sites [Suna (1970), Kobayashi and Nagakura (1972b)].

Following the development of Kobayashi and Nagakura (1972) and referring to Figure 5.1, which also shows the higher S_2 and T_2 levels populated by bimolecular collisions, we can write the population rate equations:

$$\frac{dn_1}{dt} = \alpha - \beta_1 n_1 - \beta_{1T} n_1 - 2\gamma_1 n_1^2 + \beta_2 n_2 - \gamma_{ST} n_1 n_T \qquad 5\text{-}1$$

and

$$\frac{dn_2}{dt} = \gamma_1 n_1^2 - \beta_2 n_2 \qquad 5\text{-}2$$

where n_1, n_2, and n_T are the exciton population densities of the S_1, S_2, and T_1 levels, respectively, and α is the population rate determined by the pump. If we assume that the S_2 level rapidly attains steady state ($dn_2/dt=0$), Equation 5-2 becomes:

$$n_2 = \frac{\gamma_1 n_1^2}{\beta_2}.$$

Substituting into Equation 5-1, we obtain:

$$\frac{dn_1}{dt} = \alpha - \beta_1 n_1 - \beta_{1T} n_1 - \gamma_1 n_1^2 - \gamma_{ST} n_1 n_T. \qquad 5\text{-}3$$

Similarly for the triplet state:

$$\frac{dn_T}{dt} = \beta_{1T} n_1 - \beta_T n_T - 2\gamma_T n_T^2 + \beta_{T_2} n_{T_2} - \gamma_{ST} n_1 n_T \qquad 5\text{-}4$$

and

$$\frac{dn_{T_2}}{dt} = \gamma_T n_T^2 - \beta_{T_2} n_{T_2} + \gamma_{ST} n_1 n_T. \qquad 5\text{-}5$$

Again assuming that the T_2 level rapidly attains steady state, Equation 5-5 yields:

$$n_{T_2} = \frac{\gamma_1 n_T^2 + \gamma_{ST} n_1 n_T}{\beta_{T_2}}.$$

Substituting into Equation 5-4, we obtain:

$$\frac{dn_T}{dt} = \beta_{1T} n_1 - \beta_T n_T - \gamma_T n_T^2.$$

Finally, for the S_0 level:

$$\frac{dn_0}{dt} = -\frac{dn_1}{dt} - \frac{dn_T}{dt}.$$

This set of coupled differential equations can be solved numerically. As a first approximation, we can solve Equation 5-3 by neglecting the population term, α, and the singlet-triplet annihilation term. Integration yields:

$$\frac{1}{n_1} = e^{\beta_1 t}\left(\frac{\gamma_1}{\beta_1} + \frac{1}{\eta_1}\right) - \frac{\gamma_1}{\beta_1} \qquad 5\text{-}6$$

where β_1 and β_{1T} have been combined, and η_1 is the initial population in the S_1 state just after the pump pulse. This equation is valid after the exciton population has relaxed to the bottom of the S_1 manifold assuming singlet-triplet annihilation is not a dominant decay mechanism.

MPc Thin Film Dynamics

The exciton dynamics of MPc thin films have been studied though not as extensively as in MPc solutions. In these films, as discussed in Chapter 3 and illustrated in Figures 3.2 and 3.3, the Q and Soret bands are considerably broadened from their monomer widths by intermolecular interactions. Packing the Pc molecules more densely broadens the Q band, electronic coupling and energy transfer between the Pc rings increases, and exciton decay becomes faster [Kaltbeitzel *et. al.* (1989)]. More ordered films also contribute to faster exciton migration [Casstevens *et. al.* (1990)].

While vibrational relaxation within an excited state has been quoted as occurring on a picosecond time scale in liquids, energy relaxation of excitons within the broadened singlet exciton band of a polycrystalline FAlPc thin film was seen to occur almost instantaneously (within 50 fs) in pump-probe spectroscopic experiments [Ho and Peyghambarian (1988)]. In addition, internal conversion from S_1 to S_0 was found to be very small or nonexistent in MPc solutions due to symmetry constraints [Simon and André (1985), Brannon and Magde (1980)]. In the molecular solid, however, a quasicontinuum of phonon modes exist which can support a continuous range of molecular vibrations [Trout *et. al.* (1984)]. Thus in MPc films we expect rapid nonradiative relaxation due to exciton-phonon coupling. As with MPc solutions, intersystem crossing from S_1 to T_1 increases with the size of the central metal ion in MPc thin films [Yoshino *et. al.* (1974)].

When excitons are created in a sample by optical pumping, a bleaching of the S_0 to S_1 absorption is observed. Excitons occupy the excited state thus blocking further absorption of photons and leading to an increase in transmission. The change in the absorption is proportional to the population difference between the levels. The absorption saturation signal decays as the excitons leave the S_1 state and return to the ground state. Intensity-dependent decay processes are expected to play an important role in these dynamics for optically-excited MPc films. In early photoconductivity experiments on ZnPc single crystals, a bimolecular recombination process was suggested to explain the faster carrier lifetimes observed with increasing excitation intensity [Yoshino *et. al.* (1974)]. In transient pump-probe spectroscopy experiments on an H_2Pc thin film, an exciton-exciton annihilation decay of 5.7 ps was determined for singlet excitons on adjacent lattice sites [Greene and Millard (1985a,b), Millard and Greene (1986)]. An intensity-dependent decay of a degenerate four wave mixing (DFWM) signal for an $H_2Pc(Cp)_4$ thin film was found to have two components: a rapid subpicosecond decay followed by a longer decay of about 5 ps [Prasad (1988b)]. Transient pump-probe spectroscopy experiments on an FAlPc thin film also indicated two-component exciton decay: a rapid subpicosecond intensity-dependent component and a slower few picosecond intensity-independent component [Ho and Peyghambarian (1988)]. The subpicosecond decay was attributed to bimolecular exciton-exciton annihilation, and the slower decay to exciton-phonon interaction. In DFWM experiments on evaporated films of H_2Pc and Langmuir-Blodgett films of SiPc, bimolecular decay was found to dominate the exciton dynamics at high excitation densities [Casstevens *et. al.* (1990)]. They observed more rapid decays for the more ordered SiPc films and suggested that efficient bimolecular decay and excitation transfer may be attributed to the two-dimensional, planar geometry of phthalocyanine.

Another interesting spectral feature observed after optically pumping MPc thin films is induced absorption. Induced absorption has been observed in the 450 to 550 nm region in H_2Pc and attributed to excited-state absorption [Greene and Millard (1985b), Millard and Greene (1986)]. Similar induced absorption was observed in transient differential absorption spectra of H_2Pc and CuPc solutions [McVie *et. al.* (1978)] and columnar phases of a ZnPc [Markovitsi and Lécuyer (1988), Markovitsi *et. al.* (1988)]. These groups attributed the induced absorption signal to triplet state absorption. In addition, the decay of the induced-absorption signal was attributed to bimolecular triplet-triplet annihilation [Markovitsi and Lécuyer (1988), Markovitsi *et. al.* (1988)].

Pumping our AlPc films with 620-nm and 760-nm fs pump pulses, we observe both an absorption saturation at the bottom of the excited-state manifold, as presented in Chapter 4, and an induced absorption from 480 to 620 nm.

CHAPTER 6

ABSORPTION SATURATION AND INDUCED ABSORPTION IN ALUMINUM PHTHALOCYANINE THIN FILMS

While exciton relaxation within the first excited singlet state manifold occurs on a subpicosecond time scale, as discussed in Chapter 4, relaxation between the excited singlet, triplet, and ground state manifolds occurs on picosecond and longer time scales. We have time- and wavelength-resolved the subpicosecond and few-picosecond relaxation mechanisms in our FAlPc and ClAlPc thin film samples using transient pump-probe spectroscopy. (Femtosecond studies are limited by the maximum delay capabilities of our experimental setup, ≈100 ps.)

The FAlPc thin film was pumped with 615-nm, 130-fs, 3.9-GW/cm^2 pump pulses and with 760-nm, 130-fs, 3.9-GW/cm^2 pump pulses. The ClAlPc thin film was pumped with 620-nm, 100-fs, 5.8-GW/cm^2 pump pulses. For these experiments, the pump and probe pulses were polarized parallel. Figure 6.1 indicates the changes observed in the absorption spectra when the continuum pulses probe the thin films approximately 400 fs after the pump pulses. The linear absorbance spectra and the pump spectra are shown by solid lines and the 400-fs spectra by dashed lines. There is clearly a reduction (saturation or bleaching) of the Q-band absorption peak and a broad region of increased absorption to the high energy side of the Q-band for all three cases. The maximum saturation of the absorption occurs on the low-energy edge of the Q-band.

Transient DT Spectra

Figure 6.2 shows the time evolution of the corresponding DT spectra for the 620-nm pumped FAlPc thin film. The time delays are indicated in fs, and each time delay spectrum is a composite of four DT curves taken in four separate, overlapping spectral regions. At

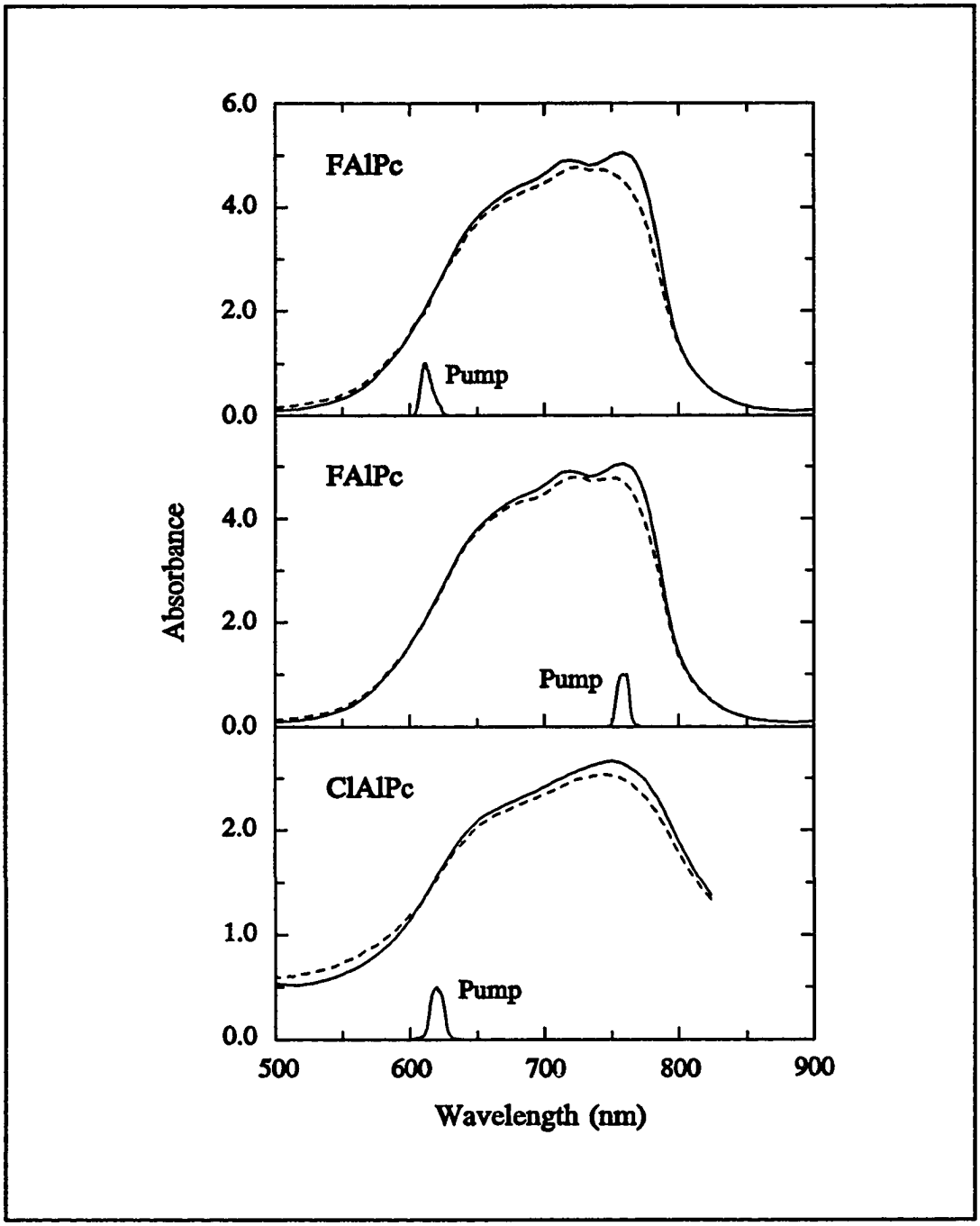

Figure 6.1 Change in absorbance spectra at 400 fs

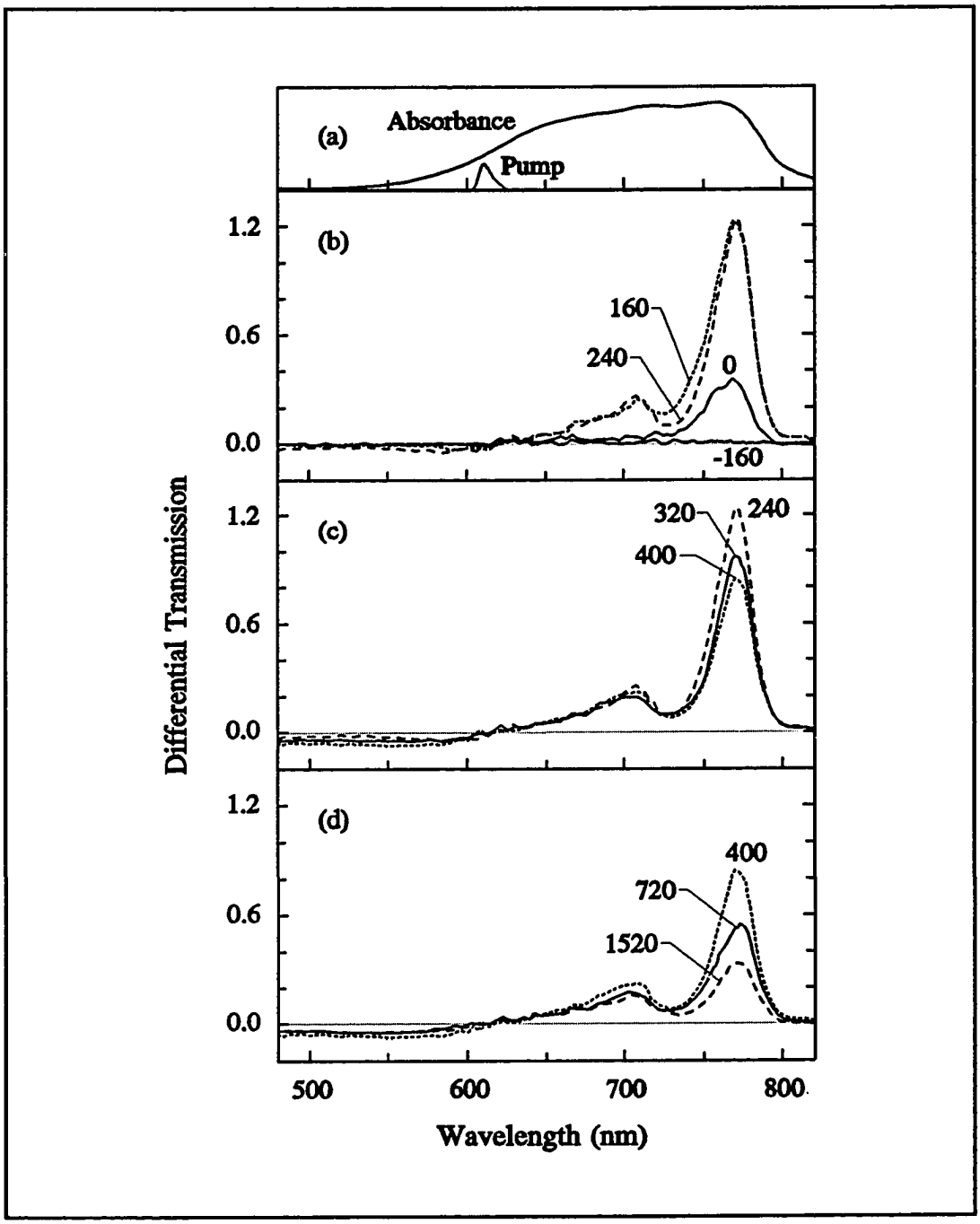

Figure 6.2 FAlPc DT spectra created by 620-nm pump

0 fs, when the pump and probe pulses are temporally overlapped, an increase in the transmission, absorption saturation (AS), is seen on the low energy side of the Q band [Fig. 6.2(b)]. When the probe lags the pump by 160 fs, the signal has maximized and a smaller AS peak becomes discernible at ≈700 nm. Eighty fs later, the large DT peak has red shifted, and a small, broad, negative signal appears at shorter wavelengths indicating a decrease in the transmission, induced absorption (IA). By 400 fs, the large AS signal has decreased by about 30% and the IA signal has maximized [Fig. 6.2(c)]. At later times, both AS and IA signals diminish [Fig. 6.2(d)].

Decay within the Q band

Clearly, the large AS signal is caused by bleaching of the optical transitions at the bottom of the Q-band by the pump-induced excitons as discussed in Chapter 4. The large spectral separation between the pump pulse and the AS signal as illustrated in Figures 6.2(a) and (b), together with the rapid onset of the AS signal, indicate a very rapid initial decay of the excitons within the Q band. This agrees with the observations of Chapter 4 where the exciton population decayed into the states at the bottom of the Q band within 120 fs after the onset of the coherent spectral hole burned by the leading edge of the pump pulse. It is interesting to note that no coherent spectral hole is observed at the 615-nm pump location in Figure 6.2(b), apparently due to very rapid relaxation mechanisms which are present when the excitation frequency is far above the exciton energy. The lack of a coherent spectral hole agrees with theoretical predictions which indicate that rapid dipole decay rates decrease the overall magnitude of hole-burning signals [Fluegel *et. al.* (1987), Lindberg and Koch (1988b), Sokoloff *et. al.* (1988)]. Small noise oscillations are observed in the spectral region of the 615-nm pump pulse for all times and are attributed to noise in the probe pulse as discussed in Chapter 2.

Vibronic transitions

The next interesting feature in the DT spectra of Figure 6.2(b) is that the maximum AS signals at 160 fs and 240 fs look remarkably similar to the FAlPc monomer absorption spectra shown in Figure 3.2, except that the AS signals are shifted to lower energy. For the monomer, the smaller amplitude, higher energy peaks are attributed to vibronic transitions. High-quality Pc crystalline thin films which have relatively narrow Q-bands also exhibit vibronic sidebands [Hoshi *et. al.* (1990)]. We must assume that these vibronic transitions also contribute to the absorption profile of polycrystalline thin films. In thin films, however, because of the many different local site environments seen by the constituent molecules, as discussed in Chapter 3, these vibronic contributions are expected to be considerably broadened and thus less noticeable in the linear absorbance spectrum. We attribute the smaller amplitude, higher energy AS peak observed in Figure 2.6 to ground-state depopulation of these vibronic transitions.

When an exciton population is excited in a molecular system, the observed change in the absorption is proportional to the population difference between the upper and lower levels of the transitions. While an exciton population residing in the S_1 level bleaches the 0-0 transition, the optically-active vibrational modes of the S_1 level also see a population difference due to the depopulation of the ground state. A small AS signal is then expected for the vibronic sidebands, i.e. the 0-1 transition. Since the population difference is smaller for a vibronic transition, the vibronic AS signal is expected to be smaller than for the 0-0 AS signal. In agreement, bleaching of the 0-0, 0-1, and 1-0 transitions has been observed in organic dye solutions; the smaller 0-1 and 1-0 vibronic AS peaks were called replica holes [Brito Cruz *et. al.* (1986), Shank *et. al.* (1986)].

The vibronic AS signal observed in Figure 6.2 appears to have several components. The separation from the main AS peak corresponds roughly to energies of 1000 to 1700 cm^{-1}.

Several strong, symmetry-allowed vibrational modes have been observed in this region in ClInPc [Aroca *et. al.* (1986)], ClGaPc [Jennings *et. al.* (1986)], and ClAlPc [Aroca *et. al.* (1987)] thin films which are structurally similar to the FAlPc thin film. It is interesting to recall that vibronic contributions were also indicated in the early-time DT spectra created by a perpendicular 760-nm pump as discussed in Chapter 4.

Decay into triplet states

We now discuss the onset of the IA signal which becomes evident in the 240 fs spectrum of Figure 6.2(b). The red-shift between the 160-fs and 240-fs AS signals appears to coincide with the appearance of the IA signal. Excitons are decaying out of the S_1 level since the total area under the AS curve is reduced between the 160-fs and 240-fs spectra. In addition, the remaining excitons are relaxing to lower energy within the S_1 manifold as evidenced by the red-shift. Since rapid, nonradiative, intersystem decay from the S_1 singlet state into the T_1 triplet state manifold is expected, as discussed in Chapter 5, it is likely that the IA signal is a result of induced absorption from the T_1 manifold.

For a linear absorption spectrum, all molecules are in the ground state, the T_1 state is unoccupied, and the one-photon allowed T_1 to T_2 transition is not observed. However, when the T_1 state becomes occupied, the triplet transition becomes allowed, and absorption increases in the triplet transition energy region resulting in an IA signal. The triplet-triplet absorption band has been observed in the 400-600 nm region in several Pcs [McVie *et. al.* (1978), Markovitsi and Lécuyer (1988), Markovitsi *et. al.* (1988)]. The location of the band varied little for different central metal ions, as expected, since the optical transitions in MPcs are attributed entirely to the Pc ring π-electron system as discussed in Chapter 3. We observe the IA signal in Figure 6.2 from <480 nm to 620 nm which clearly coincides with the documented triplet-triplet absorption band. While the possibility exists that excited-state

absorption from the S_1 state could contribute to the IA signal, the evidence presented here indicates that the IA signal is most probably caused by excited-state absorption from the triplet state manifold. For MPcs with heavier central metal ions, we would expect to see a larger IA signal and a rapidly decaying AS signal. Because of the enhanced intersystem crossing from S_1 to T_1 for heavier MPcs, as discussed in Chapter 5, the S_1 state would rapidly lose much of its population to the T_1 manifold resulting in larger IA signals.

In the 320 fs and 400 fs curves of Figure 6.2(c), the IA signal continues to grow as the AS signal continues to diminish, again, indicating an intersystem relaxation from the S_1 level to the T_1 manifold. The IA signal maximizes in the 400 fs spectra, 240 fs after the maximum IA signal, indicating that a quasi-steady state has been reached in the relaxation between the S_1, T_1, and S_0 levels. At later times [Fig. 6.2(d)], both signals diminish as the excitons relax to the ground state from both the S_1 and T_1 states.

The transient DT spectra for the 760-nm pumped FAlPc thin film are shown in Figure 6.3. The time delays are indicated in fs, and each time delay spectrum is a composite of three overlapping spectral regions. Very similar features are observed with the exception that at 0 fs [Fig. 6.3(b)], the coherent spectral hole discussed in Chapter 4 is observed. As with Figure 6.2, small probe-induced noise oscillations are observed in the 615-nm spectral region. Figure 6.3(c) shows that the IA signal increases as the AS signal decreases corresponding to intersystem crossing from S_1 to T_1. The IA signal maximizes at 400 fs, 200 fs after the maximum AS signal. At the later times shown in Figure 6.3(d), both signals dissipate. (The DT spectra for the ClAlPc thin film did not have sufficient spectral overlap to accurately assign consistent time delays to adjacent spectral regions.) To better understand the dynamics of the intermolecular decay processes discussed above, we studied the decay of the AS and IA signals as a function of time.

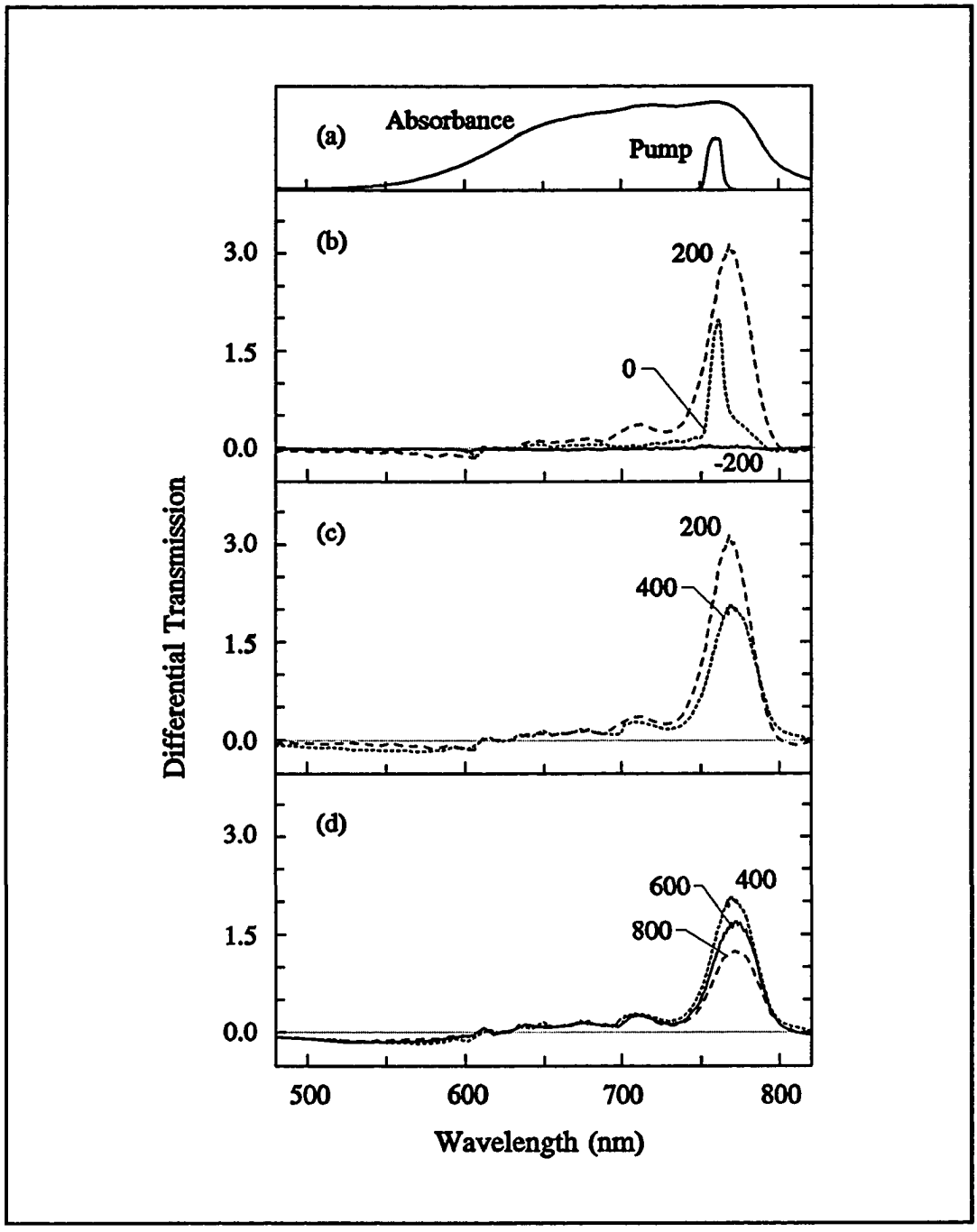

Figure 6.3 FAlPc DT spectra created by 760-nm pump

Decay Dynamics

The early-time single-wavelength decay dynamics of the AS and IA signals are shown in Figures 6.4 and 6.5, respectively. The magnitudes of the DT curves were tabulated at discrete wavelengths from the original DT data. The wavelengths were chosen to coincide with the peaks of the AS and IA signals. (Only a few of the acquired DT curves are shown in Figures 6.2 and 6.3.) Each tabulated curve was then normalized to unity and the maximum shifted to 0 ps.

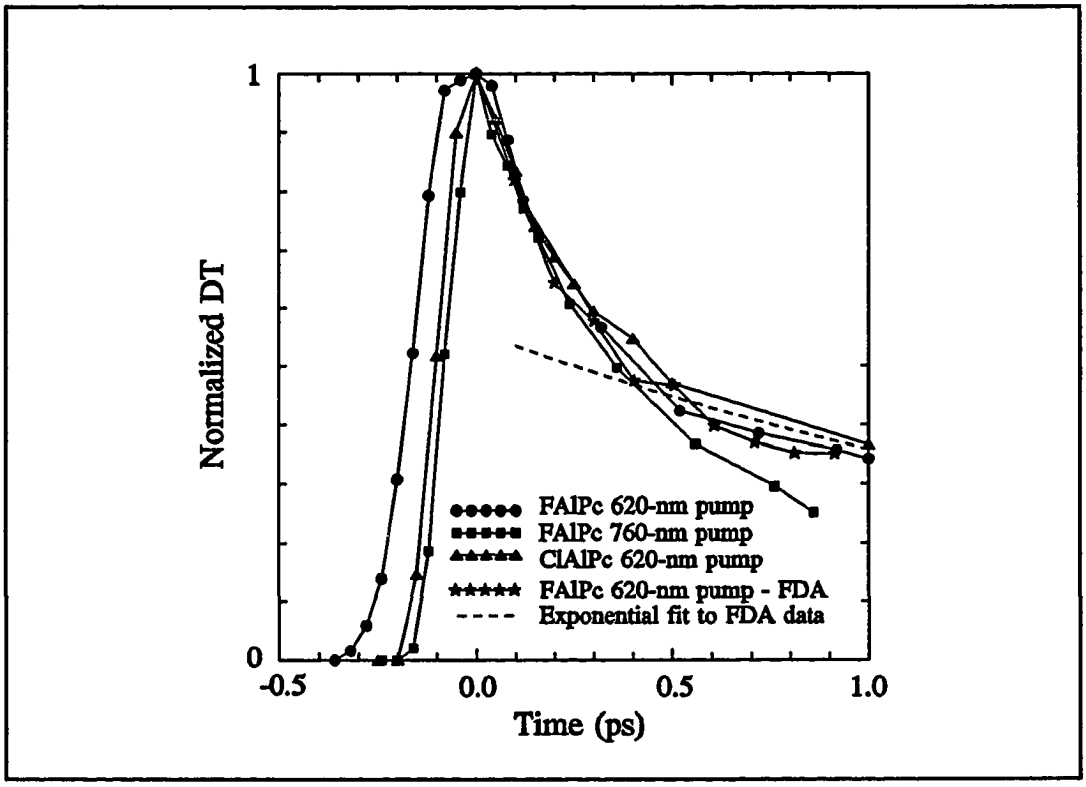

Figure 6.4 Absorption saturation decay

For the AS signals in FAlPc, the DT were tabulated at 770 nm for both the 620-nm- and 760-nm-pump cases. For the AS signal in the 620-nm pumped ClAlPc sample, the DT peak magnitude occurred at 775 nm and the data were tabulated at this wavelength. Also

shown in Figure 6.4 is a normalized decay curve acquired with the FDA system on a 620-nm pumped FAlPc thin film and the best exponential fit to that curve which yields $\tau \approx 2.2$ ps. The FDA data were acquired at 780 nm, the DT maximum for that thin film. Clearly, all four curves in Figure 6.4 deviate from mono-exponential decay at early times.

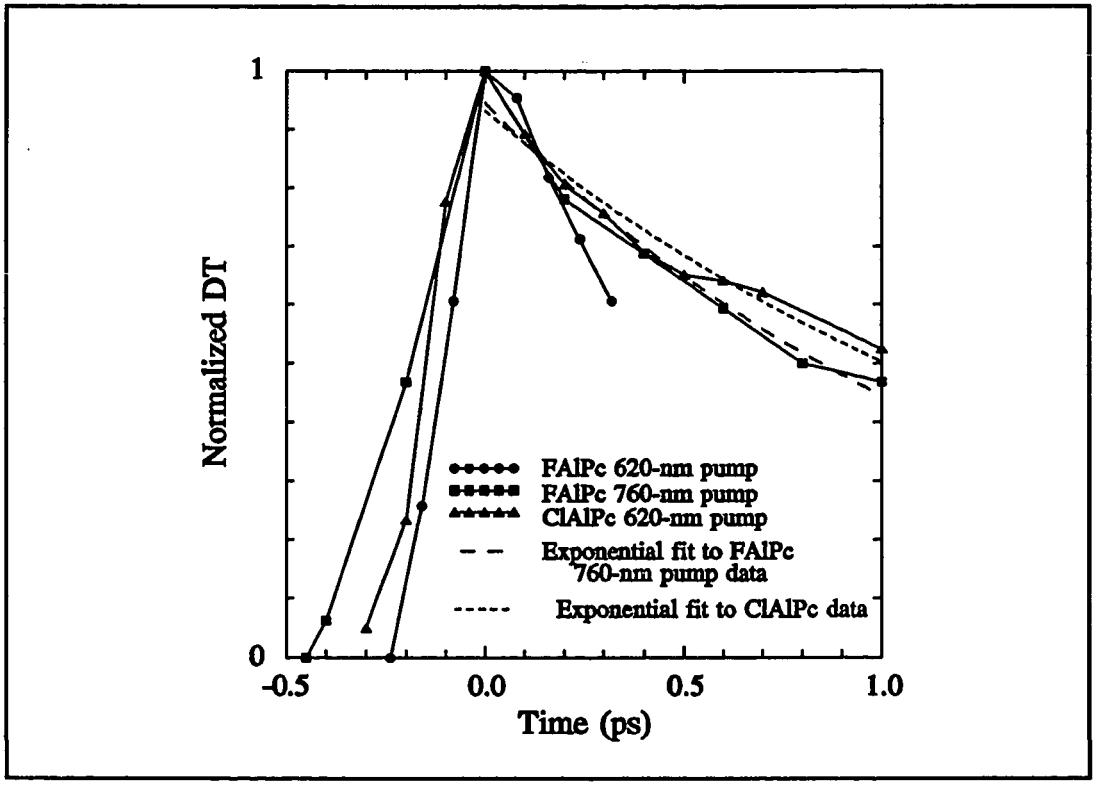

Figure 6.5 Induced absorption decay

Figure 6.5 shows the decay curves for the IA signals. All curves were tabulated at 550 nm. Because the magnitude of the IA signal is small, the large signal-to-noise ratio makes these curves unreliable at later times. Also shown are the best exponential fits to the 760-nm pumped FAlPc curve and the 620-nm pumped ClAlPc curve. These fits yield $\tau \approx 1.3$ ps and $\tau \approx 1.6$ ps for FAlPc and ClAlPc, respectively. Unlike the AS signals, these signals appear to deviate only slightly from exponential behavior. Reproducible FDA curves

have not yet been obtained in this region, again, because of the small magnitude of the signal.

The deviation from mono-exponential decay of the AS signal at early times indicates that bimolecular decay processes may be significant, as discussed in Chapter 5. The near-exponential decay of the IA signal indicates that unimolecular processes are probably dominant though some bimolecular decay may be present at very early times. Since we do not observe any phosphorescence from the triplet state, the triplet decay to the ground state is dominantly nonradiative. To quantify the bimolecular behavior of the AS curves, we must relate the measured DT magnitudes to the theoretically-definable population levels discussed in Chapter 5.

Simple Bimolecular Decay Theory

From two-level theory, we know that absorption is proportional to the population difference between the upper and lower levels, $\alpha L = K (n_1 - n_0)$, where 1 and 0 signify the upper and lower levels, respectively, and n represents the percentage of the molecular population in the level. Recalling that for the linear absorption, all molecules are in the ground state, n_1=0 and n_0=1, K=-α_0L, and the absorbance becomes $\alpha L = -\alpha_0 L N$, where N represents the population difference n_1-n_0. It follows that $\Delta\alpha L = -\alpha_0 L\ \Delta N$. To relate the change in the population difference, ΔN, to DT, we recall that

$$DT = \frac{T - T_0}{T_0} = \frac{e^{-\alpha L} - e^{-\alpha_0 L}}{e^{-\alpha_0 L}} = e^{-\Delta\alpha L} - 1.$$

Substituting the expression for $\Delta\alpha L$, this becomes

$$DT = e^{\alpha_0 L \Delta N} - 1. \qquad 6\text{-}1$$

If we assume that only a small percentage of the excited molecules cross into the triplet manifold, we can say that $n_0 + n_1 \approx 1$. Then

$$\Delta N = (n_1 - n_0)_{final} - (n_1 - n_0)_{initial} = (2n_1 - 1) - (-1) = 2n_1$$

since the initial state corresponds to the linear absorption. Substituting ΔN and the expression for n_1 derived in Chapter 5 (Equation 5-6) into Equation 6-1, we obtain

$$DT = \exp\left[\frac{2\alpha_0 L}{e^{\beta_1 t}\left(\frac{\gamma_1}{\beta_1} + \frac{1}{\eta_1}\right) - \frac{\gamma_1}{\beta_1}}\right] - 1. \qquad 6\text{-}2$$

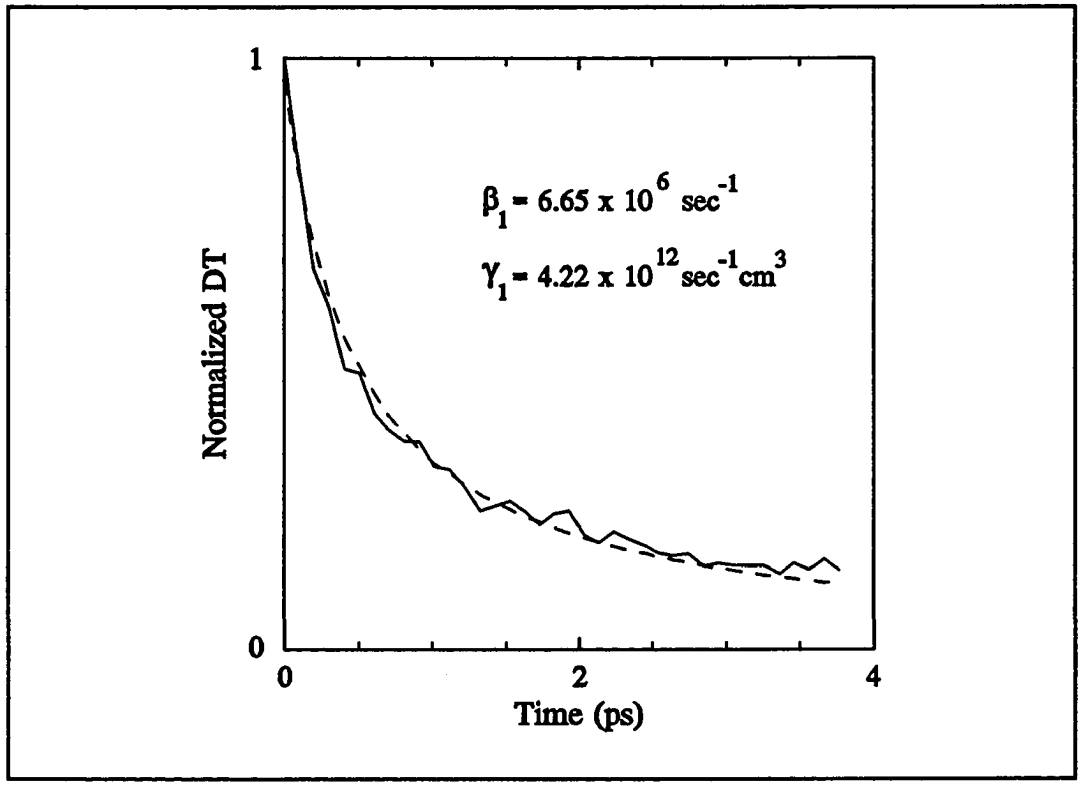

Figure 6.6 Theoretical fit to absorption saturation decay curve

This expression was fit to the AS decay curve obtained with the FDA system for a 620-nm pumped FAlPc sample using the least χ^2 fitting algorithm of Marquardt [Bevington (1969)]. The results are shown in Figure 6.6; the FDA decay curve is shown with a solid line and the best fit indicated by the dashed line. The fit yielded a unimolecular rate constant,

β_1=6.65x10^6 sec^{-1}, and a bimolecular rate constant, γ_1=(4.22±.02)x10^{-12} sec^{-1} cm^3. β_1 could be varied by almost an order of magnitude with little resulting change in γ_1. In the 4-ps time domain of this fit, τ_1=1/β_1=150 ns is expected to have little effect on the fit. The good agreement between the data and this simple theory indicates that bimolecular decay is a prominent decay mechanism from the S_1 state. This implies that effective singlet exciton migration occurs in the molecular lattice, most likely due to efficient electronic coupling between molecules. A small bimolecular decay component may be present at very early times for the IA signal though this is difficult to quantify since the signal to noise ratio is poor for this data. Since bimolecular decay processes are density dependent, a small or nonexistent triplet bimolecular decay component indicates that only a small percentage of the singlet excitons relax to the triplet manifold. The relatively small size of the IA signal also indicates that a small percentage of the singlet excitons relax into the triplet manifold.

The information presented here helps us to understand the optical nonlinearity decay mechanisms of organic Pc molecules. This understanding will allow us to design more effective all-optical organic switching devices. In particular, rapid bimolecular decay can be exploited to increase switching speed while decay into slower triplet states should probably be minimized for optimal devices. We discuss the demonstration of an all-optical switching device using a guest-host organic polymer in the following chapter.

CHAPTER 7

PICOSECOND ALL-OPTICAL ORGANIC ETALON SWITCH

There is growing interest in using nonlinear optical materials for photonic devices. Nonlinear optical materials may potentially be used in a variety of optical operations, such as frequency conversion, high-speed optical switching, and optical signal processing [Gibbs *et. al.* (1990)]. The basic requirement of a practical device is to find a material which has a large nonlinear optical effect and a fast response time. Nonlinear organic materials, because of their π-electron cloud, have rapid nonlinear response times. Nonlinear organic materials are potentially useful for applications in all-optical serial processing of high bit-rate data streams [Stegeman *et. al.* (1989)].

Optical bistability has been reported in Fabry-Perot cavities filled with organic liquids such as CS_2 and nitrobenzene [Bischofberger and Shen (1979)], a BDN dye solution [Zhu and Garmire (1983)], and a silicon naphthalocyanine thin film [Garito and Wu (1989)]. A Kerr interferometric NOR logic gate was demonstrated using a 4BCMU-polydiacetylene solution [Ho *et. al.* (1986)], and bistable behavior was observed in poly-4BCMU quasi-waveguides. However, an ultrafast nonlinear optical logic gate using an organic thin film in an etalon has not been demonstrated. Here we report the switching characteristics of such a nonlinear etalon logic NOR gate constructed with a guest-host organic thin film, 7-[4-[(4-hexyloxyphenyl)azo](naphthyl)azo-(2,3-dihydro-1,3-dimethyl-2-octyl)] perimidine (DNP) doped in poly(methyl methacrylate) (PMMA), or DNP/PMMA, sandwiched between two partially reflecting mirrors [Williams *et. al.* (1990)]. DNP is a newly-developed organic molecule created by researchers at Hercules Incorporated.

Nonlinear etalons can perform various optical logic operations such as AND, OR, and NOR [Jewell *et. al.* (1985)]. A combination of NOR gates can produce all binary logic

functions. The principle of such operations is the shifting of the Fabry-Perot transmission peak in response to an optical control pulse. The control pulse changes the refractive index of the nonlinear material at the wavelength of the probe pulse. This shifts the transmission peak thus changing the transmission of the probe pulse through the etalon. For example, if the probe is initially tuned to a high transmission peak, a shift of the peak will decrease the probe transmission and result in a NOR gate operation. The physical origin of the refractive index change may originate from different mechanisms in different types of materials. For example, carrier-induced many-body effects [Migus *et. al.* (1985)] and the optical Stark effect [Hulin *et. al.* (1986), Jin *et. al.* (1990)] were the origin of nonlinear optical gating in GaAs multiple quantum well etalons and waveguides. Two-photon absorption effects induced switching in polydiacetylene-based directional couplers [Townsend *et. al.* (1989)].

Bulk DNP Dye Doped in PMMA

Our guest-host organic DNP/PMMA thin film was prepared by dissolving DNP (10% by weight of PMMA) and PMMA in tetrahydrofuran and spin-coating onto a glass substrate. The molecular structure of DNP and the linear absorbance spectrum of the resulting 1-μm-thick thin film are shown in Figures 7.1 and 7.2, respectively. The absorption peak at ≈600 nm is due to the first π-π^* electronic transition of the guest DNP molecule, broadened by vibronic coupling. The host PMMA polymer is transparent in the spectral region displayed in Figure 7.2.

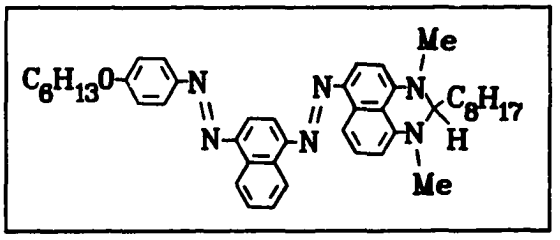

Figure 7.1 Molecular structure of DNP

The nonlinearity of the DNP/PMMA thin film was examined using ultrafast pump-probe spectroscopy. The film was pumped near the peak of the absorption with 80-fs, ≈1-GW/cm^2, 615-nm pump pulses, as illustrated in Figure 7.2. (The pump is shown in

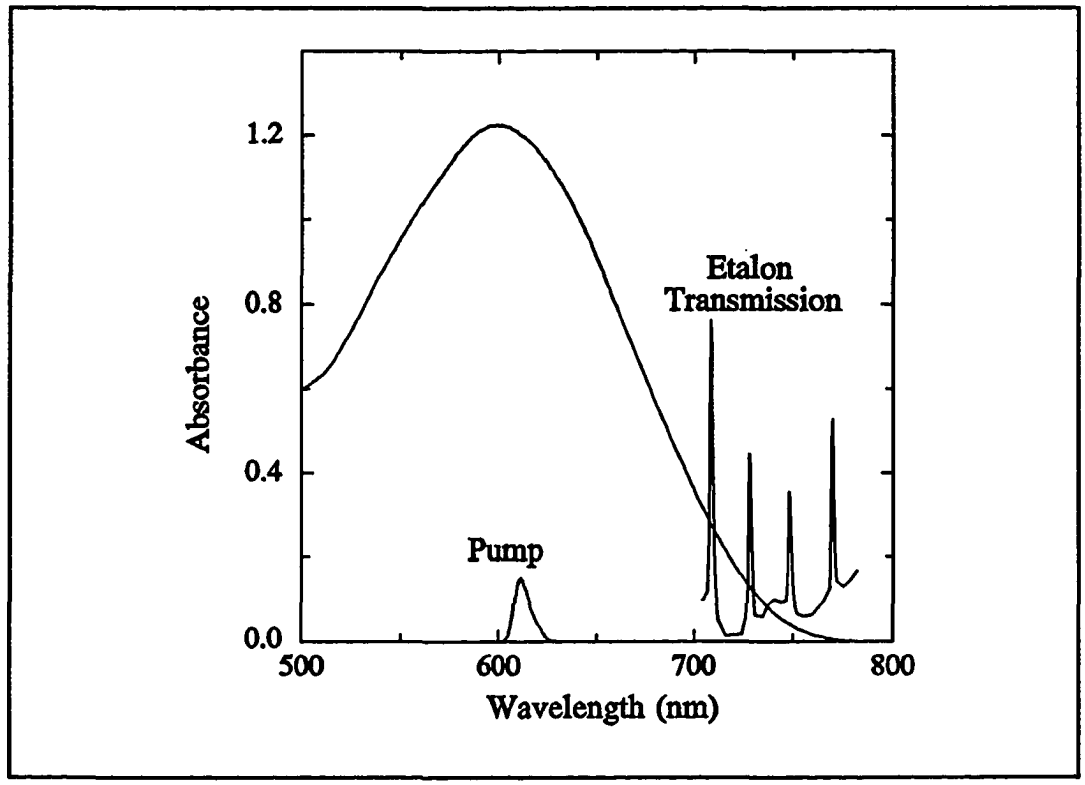

Figure 7.2 Absorbance spectrum of DNP/PMMA thin film

arbitrary units.) Figure 7.3 displays the measured DT spectra at three time delays: 100 fs, 1 ps, and 5 ps. The positive DT signal indicates an increase in the probe transmission. This bleaching maximizes in ≈100 fs and decays rapidly. The 5-ps spectrum shows that most of the induced bleaching has recovered. The DT signal did not completely recover after our maximum delay of ≈100 ps. This slower recovery may be due to decay from long-lived triplet states. The oscillatory structure in the 100-fs spectrum around the pumping wavelength may be related to the transient oscillations that have been previously observed in organic dyes [Shank *et. al.* (1986), Brito Cruz *et. al.* (1986, 1988)] and in inorganic semiconductors [Fluegel *et. al.* (1987), Joffre *et. al.* (1988), Sokoloff *et. al.* (1988)]. These oscillations are usually observed at negative time delays. Due to the uncertainty in

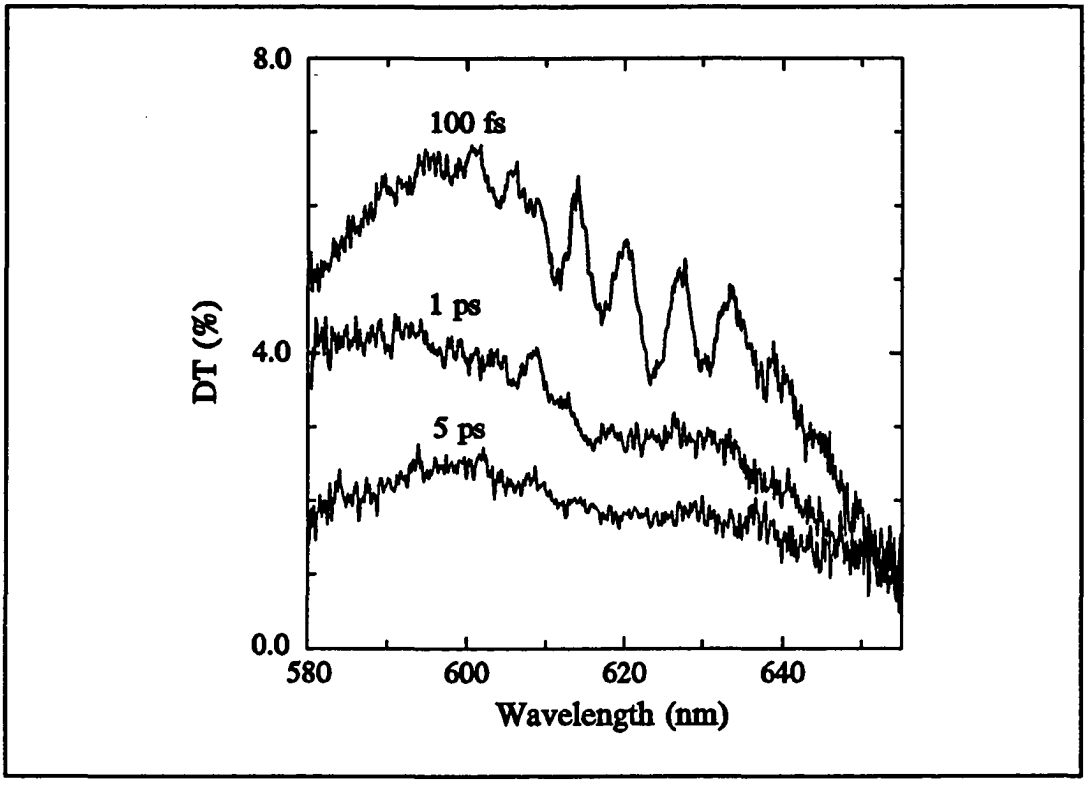

Figure 7.3 DT spectra of DNP/PMMA thin film

determining "zero" time, as discussed in Chapter 2, it is possible that our 100 fs curve may actually correspond to a negative time delay. The fast decay of the DT signal is attributed to the rapid nonradiative lifetime of the DNP molecule.

Fabry-Perot Etalon Logic Gate

A nonlinear etalon was formed by placing the DNP/PMMA thin film between two partially reflecting mirrors. The thin film was deposited onto a dielectric-coated substrate and the second mirror attached with optical adhesive to complete the device. The mirrors were >95% reflective between 700 nm and 820 nm and nearly transparent at 610 nm. This choice of mirror reflectivity was adopted to enhance the efficiency of the device:

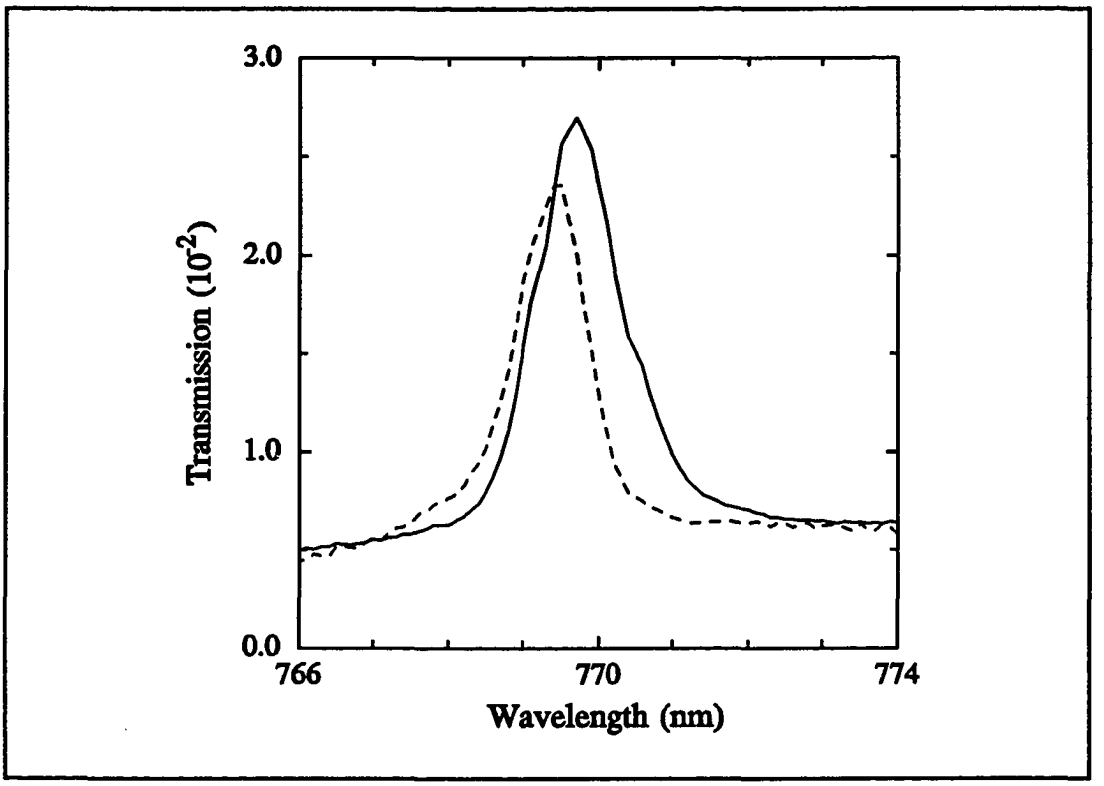

Figure 7.4 Shift of Fabry-Perot peak

transparent at the control (or pump) wavelength, λ=615 nm, and reflective at the probe wavelengths. The transmission of the probe through the etalon (shown in arbitrary units in Figure 7.2) indicates the spectral positions of the Fabry-Perot peaks. The free spectral range and the bandwidth of the Fabry-Perot etalon were 21.6 nm and 1.35 nm, respectively, giving a cavity finesse of 16. The continuous curve in Figure 7.4 shows the linear transmission of one of the Fabry-Perot peaks, spectrally located on the low-energy side of the absorption peak. The dashed curve in Figure 7.4 displays the same Fabry-Perot peak, 100 fs after excitation with an $\approx$1.5 GW/cm^2 pump pulse. (The damage threshold is $\approx$2.7 GW/cm^2.) The blue shift of the Fabry-Perot peak is clearly observed. This is consistent with the nonlinearity measurement of Figure 7.3 which shows a bleaching of the absorption resonance.

Absorption bleaching induces a negative index change below the resonance thus causing a blue shift of the Fabry-Perot peak ($m\Delta\lambda=2\Delta nd$ where λ is wavelength, n is refractive index, d is the thickness of the Fabry-Perot, and m is the order of the Fabry-Perot peak).

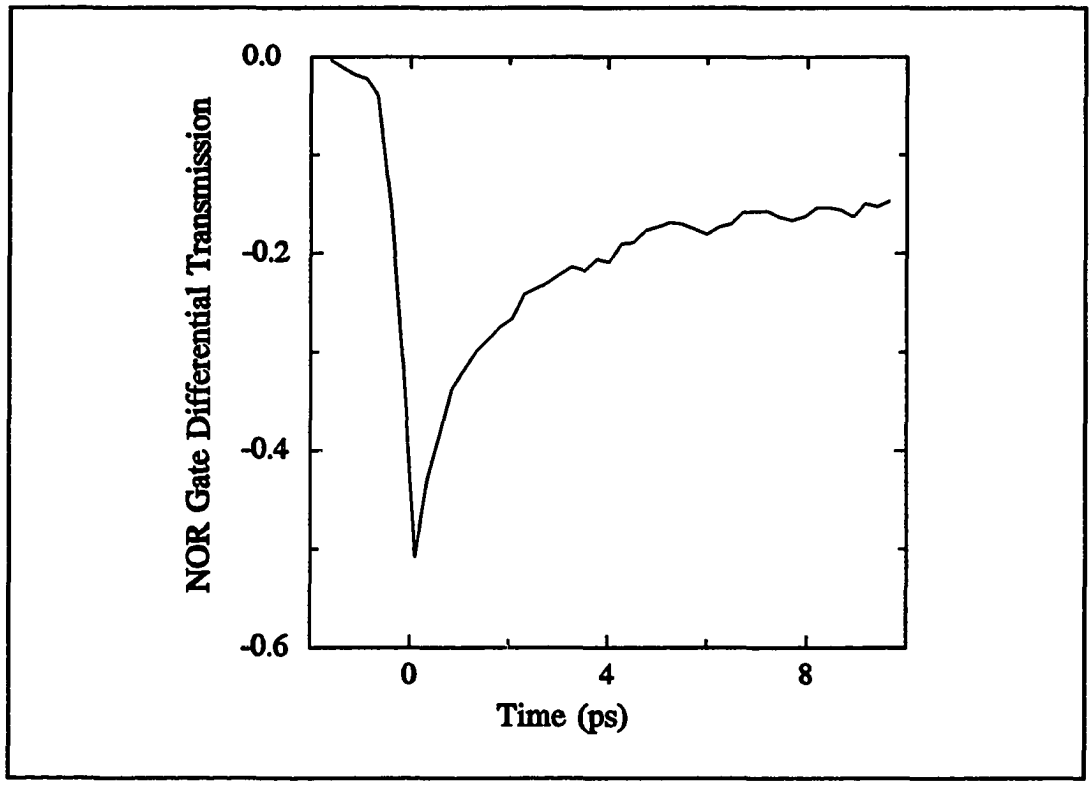

Figure 7.5 Dynamics of all-optical NOR gate at 770.3 nm

A logic NOR gate was demonstrated by probing the etalon at the wavelength where the maximum change in the transmission of the Fabry-Perot peak was observed ($\lambda_{probe}\approx$770.3 nm). The DT of the device at this wavelength was measured as a function of time delay between the pump and the probe pulses using the FDA system. The dynamics of the NOR gate are illustrated in Figure 7.5. Since an index change occurs concurrently with the bleaching of the transition, the switch-on time of the gate should be limited by the cavity build-up time: $2nd/[(1-R)c]\approx$500 fs where nd is the cavity optical path length and R is the

effective mirror reflectivity. ($R \approx 0.82$ was calculated from the measured finesse.) The measured subpicosecond switch-on of the NOR gate is in agreement with this analysis. The recovery of the signal exhibits a fast, ≈4-ps component, and slower components. The fast component is attributed to the rapid nonradiative lifetime of the DNP molecules while the origin of the slower components is not clear at present. A maximum contrast ratio of ≈2 between the switching states was observed. (A contrast ratio of ≈1.7 was observed at the adjacent Fabry-Perot peak.) From the ≈3-Å blue shift of the Fabry-Perot peak, we estimate an index change of $\Delta n \approx 0.005$ for the 1.5 GW/cm^2 pump intensity employed in the measurement.

This demonstration of a simple all-optical NOR gate using an organic etalon can certainly be refined and optimized in future organic devices. Future directions for nonlinear optical research on organic materials are discussed in Chapter 8.

CHAPTER 8

CONCLUSIONS AND FUTURE DIRECTIONS

In this manuscript, ultrafast optical nonlinearities in solid-phase organic materials have been studied using pulsed, femtosecond laser technology. In particular, after pumping the Q-band of an FAlPc thin film with parallel-polarized fs-duration pump and probe pulses, we observed coherent coupling effects which evolved into a nonequilibrium exciton population. These effects were not observed with perpendicularly-polarized pump and probe pulses indicating an effective decoupling of orthogonal polarization states in FAlPc molecules. The nonequilibrium exciton population then rapidly relaxes to the bottom of the π-π^* manifold. The singlet excitons exhibit rapid bimolecular decay at early times. In addition, some singlet excitons relax into the triplet manifold inducing excited-state triplet-triplet absorption. The triplet excitons appear to decay dominantly through nonradiative unimolecular processes, though more work is required for a full understanding of the triplet processes.

A theory is currently under development to model the coherent coupling and relaxation effects observed in Pc thin films. The application of this theory to the results presented here, however, is limited by the polycrystalline nature of the thin film samples. To obtain functional results with theoretical models, the molecular system under study must be well defined. To this end, well-characterized single crystal Pc films are currently being deposited using organic/inorganic molecular beam epitaxy (O/I-MBE) techniques [Nebesny *et. al.* (1991)]. Figure 8.1 shows the relatively narrow absorbance spectrum of an O/I-MBE-grown single crystal InPc-Cl thin film [Nebesny *et. al.* (1991)] and the much broader spectrum for the polycrystalline FAlPc thin film studied in this manuscript. The comparison of future femtosecond experiments on these single crystal Pc thin films with theoretical

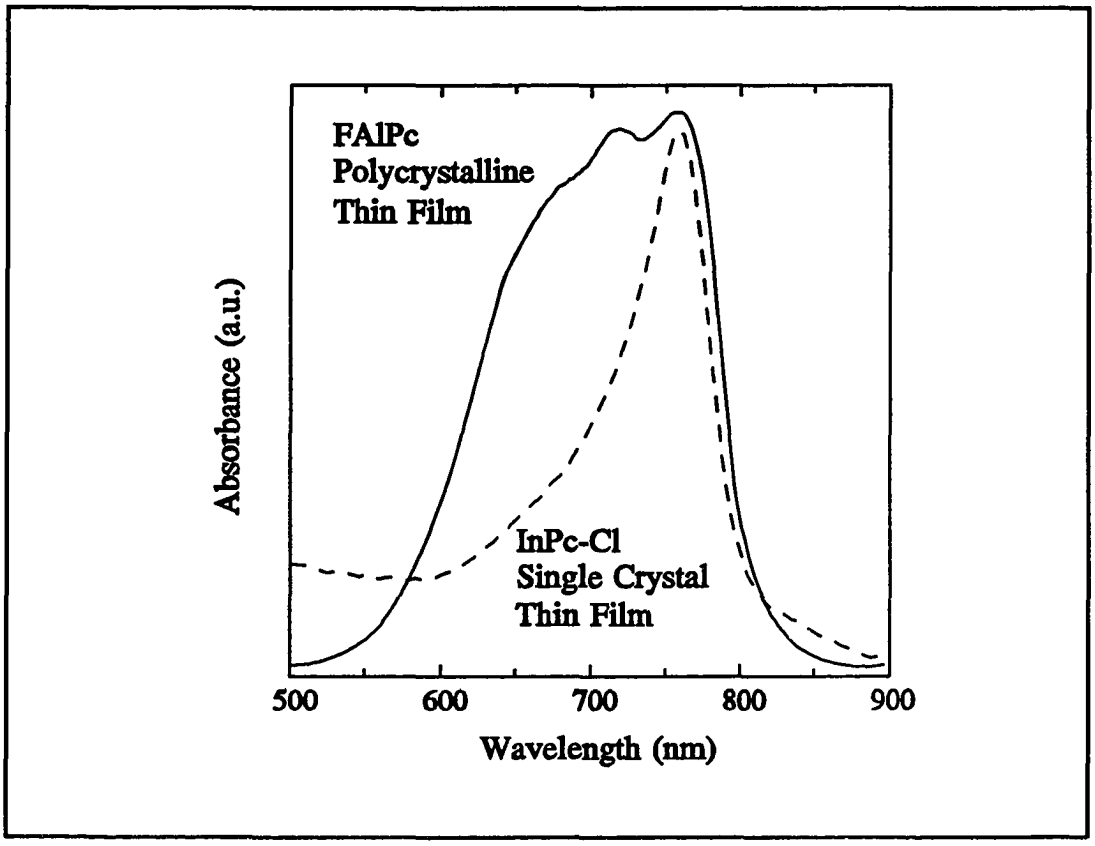

Figure 8.1 Absorbance spectra of polycrystalline and single crystal Pcs

predictions should yield valuable insight into the physical origin of optical nonlinearities in organic materials.

At this point in time, the use of organic materials in nonlinear optical and electro-optical devices is limited by the integrity of the materials themselves. This is true for inorganic semiconductors as well. A simple etalon logic gate employing an organic thin film as the nonlinear medium was demonstrated in this manuscript. The first step towards the optimization of such devices is to develop and synthesize organic materials of suitable structural quality with desirable mechanical, electrical, chemical, and nonlinear optical

properties. The headway gained by future research directed towards this goal will ultimately determine the fate of optically-nonlinear organic materials for useful device applications.

APPENDIX A

DECHIRPING PROGRAM

```
'$DYNAMIC
'       CHIRP.BAS

'       This program removes parabolic chirp.

'       The second (squared) term of the chirp parabola (wavelength
'       vs. time) should be negative.

'        BE CAREFUL!  This program is not perfectly general.

'         -- Dechirps files which have wavelength values (in nm) in
'            the first column and DTS values in the second column.

'            The files to be dechirped should be numbered
'            consecutively and named FILExx.DAT where xx is the
'            consecutive number, and the time delay between
'            successive files should be constant.

'            Up to 30 files can be dechirped at a time.

'            The program assumes that the wavelength is in nm.
'            If angstroms were used, substitute angstroms values for
'            nm values.

'            'Dechirped' files are named F????.DAT where ????
'            is the computed time delay for that curve.

'-----------------------------------------------------------------------

CLEAR , 64000!: CLOSE : CLS : KEY OFF
DIM ARRAY(1025, 30)
DIM Y(1025), LAMDA(1025)
DEF FNRECN (WL) = INT((WL - MAXL) / (MINL - MAXL) * 1023 + 1.5)
DEF FNSTRIP$ (NUM) = RIGHT$(STR$(NUM), LEN(STR$(NUM)) - 1)
DEF FNTRIM$ (NUM) = LEFT$(STR$(NUM), LEN(STR$(NUM)) - 1)
T1$ = TIME$
PRINT "     PARABOLIC-CHIRP REMOVAL PROGRAM"
PRINT
PRINT
```

```
        ' Get information on files to be dechirped

        PTH1$ = "D:\CHIRP\DATA"
5       PRINT "Path for MS-DOS files saved on the OMA ["; PTH1$;
        INPUT "]: ", PPTH1$
        IF PPTH1$ = "" THEN GOTO 410 ELSE PTH1$ = PPTH1$
410     IF RIGHT$(PTH1$, 1) <> "\" THEN PTH1$ = PTH1$ + "\"
        PRINT "Path for 'dechirped' files ["; PTH1$;
        INPUT "]: ", PTH2$
        IF PTH2$ = "" THEN PTH2$ = PTH1$: GOTO 460
        IF RIGHT$(PTH2$, 1) <> "\" THEN PTH2$ = PTH2$ + "\"
460     INPUT "First MS-DOS file (FILExx.DAT)  xx=: ", FIN
        FLN1$ = FNSTRIP$(FIN)
        FLIN$ = PTH1$ + "FILE" + FLN1$ + ".DAT"
        PRINT "Time delay (in fs) for first file "; FLIN$;
        INPUT ": ", TIME1
        PRINT "Wavelength (in nm) corresponding to "; TIME1; "fs delay: ";
        INPUT "", NOCHIRP
        INPUT "Time delay (in fs) between successive files [50]: ", DELTAT$
        IF DELTAT$ = "" THEN DELTAT = 50 ELSE DELTAT = VAL(DELTAT$)
        INPUT "Number of files to dechirp: ", CNUM
        PRINT
        PRINT "Enter the parabolic chirp coefficients:"
        PRINT "dt/d(lamda) = C + K * (lamda)"
        INPUT "C = ", C1
        INPUT "K = ", C2
        PRINT
        INPUT "Are these parameters correct?", A$: PRINT
        IF A$ = "y" OR A$ = "Y" THEN GOTO 30 ELSE GOTO 5

        ' Load the DTS files into the array for chirp removal
30      PRINT "Loading files into an array for chirp removal...": PRINT

        FLN1$ = FNSTRIP$(FIN)
        FLIN$ = PTH1$ + "FILE" + FLN1$ + ".DAT"
        OPEN FLIN$ FOR INPUT AS #1
        DTSMAX = 0: DTSMIN = 0
        N = 1
        I = 1
        DO UNTIL EOF(1)
        INPUT #1, LAMDA(I), ARRAY(I, N)
        IF ARRAY(I, N) > DTSMAX THEN DTSMAX = ARRAY(I, N)
        IF ARRAY(I, N) < DTSMIN THEN DTSMIN = ARRAY(I, N)
        I = I + 1
        LOOP
        FIN = FIN + 1
        CLOSE #1
        NPTS = I - 1
```

```
        FOR N = 2 TO CNUM
        FLN1$ = FNSTRIP$(FIN)
        FLIN$ = PTH1$ + "FILE" + FLN1$ + ".DAT"
        OPEN FLIN$ FOR INPUT AS #1
        FOR J = 1 TO NPTS
        INPUT #1, X, ARRAY(J, N)
        IF ARRAY(J, N) > DTSMAX THEN DTSMAX = ARRAY(J, N)
        IF ARRAY(J, N) < DTSMIN THEN DTSMIN = ARRAY(J, N)
        NEXT J
        FIN = FIN + 1
820     CLOSE #1
        BEEP
        NEXT N
        PRINT "Loading complete."
        PRINT

        ' Find the wavelength extrema and step size

        MAXL = LAMDA(1)
        MINL = LAMDA(NPTS)
        STEP1 = (MAXL - MINL) / NPTS
        PRINT "MAX WAVELENGTH= "; MAXL; "MIN WAVELENGTH= "; MINL
        PRINT "STEP SIZE= "; STEP1
        PRINT "MINIMUM DTS= "; DTSMIN; "   MAXIMUM DTS= "; DTSMAX: PRINT

        IF NOCHIRP > MAXL THEN GOTO 10
        IF NOCHIRP < MINL THEN GOTO 10 ELSE GOTO 20
10      PRINT "The chosen wavelength is not within the spectral region of the DTS curves."
        PRINT "Wavelength (in nm) corresponding to "; TIME1; "fs delay:  ";
        INPUT "", NOCHIRP: PRINT

20      COUNT1 = FNRECN(NOCHIRP)
        FLL$ = PTH2$ + "FILE"
        OUTNUM = TIME1

        ' Begin removing Chirp

        BEEP: BEEP
        PRINT "Removing chirp..."
        PRINT

        GOSUB 1730          'Set y() = 0; Open first file

        M = 1
1390    T = M
        B = 1
        COUNT = COUNT1
        X = 0
```

```
        GOSUB 1760    'Remove chirp

        T = M
        B = -1
        COUNT = COUNT1
        X = 0
        GOSUB 1760

1610    GOSUB 1850                    'Save y() to file
        IF M = CNUM THEN GOTO 1680
        OUTNUM = OUTNUM + DELTAT
        GOSUB 1730                    'Reset y() = 0; Open next file
        M = M + 1
        GOTO 1390

1680    PRINT : PRINT "Curves dechirped around "; NOCHIRP; " nm.": PRINT
        PRINT "Normal termination."
        T2$ = TIME$: PRINT T1$, T2$
        BEEP: BEEP

        '           GRAPHICS
        SCREEN 2
        CLS
        VIEW (20, 2)-(620, 172), , 1
        WINDOW (MINL, DTSMIN)-(MAXL, DTSMAX)

        FOR N = 1 TO CNUM

        PSET (LAMDA(1), ARRAY(1, N))
        FOR S = 1 TO NPTS
        LINE -(LAMDA(S), DTS(S, N))
        NEXT S
        NEXT N

        END    ' End of program

1730    '       Reset Y-values to zero; open output files

        FOR KNT% = 0 TO NPTS
        Y(KNT%) = 0                   ' Reset y-values to zero
        NEXT KNT%

        IF OUTNUM>=0 THEN ONN$=FNSTRIP$(OUTNUM) ELSE
           ONN$=STR$(OUTNUM)
        IF OUTNUM <=-1000 THEN FLL$ = PTH2$ + "FIL" ELSE FLL$ = PTH2$ + "FILE"
        FF$ = FLL$ + ONN$ + ".DAT"
        OPEN FF$ FOR OUTPUT AS #3
        RETURN
```

```
      '     Chirp Removal Algorithm

1760  IF T = CNUM THEN B = -1: RETURN
      IF T = 1 AND B = -1 THEN RETURN
1770  CHIRP = ABS(DELTAT / (C1 + C2 * LAMDA(COUNT)))
      Y(COUNT) = (X/CHIRP) * (ARRAY(COUNT, T+B) - ARRAY(COUNT, T))
            + ARRAY(COUNT, T)
      IF X > CHIRP THEN T = T + B: X = 0: GOTO 1760
      IF COUNT = 1 AND B = 1 THEN RETURN
      IF COUNT = 1024 AND B = -1 THEN GOTO 1610
      X = X + STEP1
      COUNT = COUNT - B
      GOTO 1770

1850  '     Record corrected data to files

      FOR A = 1 TO NPTS
      PRINT #3, LAMDA(A), Y(A)
      DTS(A, M) = Y(A)
      NEXT A
      PRINT FF$; " processed..."
      CLOSE #3
      RETURN
```

REFERENCES

G.P. Agrawal, C. Cojan, and C. Flytzanis, "Nonlinear optical properties of one-dimensional semiconductors and conjugated polymers," Phys. Rev. B 17, 776 (1978).

R.R. Alfano and P.P. Ho, "Self- and coupled-phase modulations of ultrashort laser pulses," Opt. News August, 13 (1989).

N.R. Armstrong, private communication (1990).

R. Aroca, C. Jennings, R.O. Loutfy, and A.-M. Hor, "Structure of organic thin films: Raman polarization studies," J. Phys. Chem. 90, 5255 (1986).

R. Aroca, C. Jennings, R.O. Loutfy, and A.-M. Hor, "Raman spectra of thin solid films - VI. Davydov splitting," Spectrochimica Acta 43A, 725 (1987).

R. Aroca, R.E. Clavijo, C.A. Jennings, G.J. Kovacs, J.M. Duff, and R.O. Loutfy, "Vibrational spectra of lutetium and ytterbium bis-phthalocyanine in thin solid films and SER(R)S on silver island films," Spectrochimica Acta 45, 957 (1989).

R. Aroca, Z.Q. Zeng, and J. Mink, "Vibrational assignment of totally symmetric modes in phthalocyanine molecules," J. Phys. Chem. Solids 51, 135 (1990).

W.R. Barger, A.W. Snow, H. Wohltjen, and N.L. Jarvis, "Derivatives of phthalocyanine prepared for deposition as thin films by the Langmuir-Blodgett technique," Thin Solid Films 133, 197 (1985).

P.C. Becker, H.L. Fragnito, R.L. Fork, F.A. Beisser, and C.V. Shank, "Generation of tunable 9 femtosecond pulses in the near infrared," in *Ultrafast Phenomena VI*, ed. by T. Yajima, K. Yoshihara, C.B. Harris, and S. Shionoya (Springer-Verlag, Berlin, 1988) p. 12; also Appl. Phys. Lett. 54, 411 (1989).

F.A. Beisser, "Preparation of thin nozzle for colliding pulse modelocking laser," unpublished (1981).

A. Bergman, M. Levine, and J. Jortner, "Collision ionization of single excitons in molecular crystals," Phys. Rev. Lett. 18, 593 (1967).

P.R. Bevington, *Data Reduction and Error Analysis for the Physical Sciences* (McGraw-Hill, New York, 1969), pp. 237-240.

T. Bischofberger and Y.R. Shen, "Nonlinear Fabry-Perot filled with CS_2 and nitrobenzene," Opt. Lett. 4, 40 (1979).

J.H. Brannon and D. Magde, "Picosecond laser photophysics. Group 3A phthalocyanines," J. Amer. Chem. Soc. 102, 62 (1980).

C.H. Brito Cruz, R.L. Fork, W.H. Knox, and C.V. Shank, "Spectral hole burning in large molecules probed with 10 fs optical pulses," Chem. Phys. Lett. 132, 341 (1986).

C.H. Brito Cruz, J.P. Gordon, P.C. Becker, R.L. Fork, and C.V. Shank, "Dynamics of spectral hole burning," IEEE J. Quant. Electron. 24, 261 (1988).

J.P Byrne, E.F. McCoy, and I.G. Ross, "Internal conversion in aromatic and N-heteroaromatic molecules," Aust. J. Chem. 18, 1589 (1965).

G.M. Carter, M.K. Thakur, Y.J. Chen, and J.V. Hryniewicz, "Time and wavelength resolved nonlinear optical spectroscopy of a polydiacetylene in the solid state using picosecond dye laser pulses," Appl. Phys. Lett. 47, 457 (1985).

G.M. Carter, J.V. Hryniewicz, M.K. Thakur, Y.J. Chen, and S.E. Meyler, "Nonlinear optical processes in a polydiacetylene measured with femtosecond duration laser pulses," Appl. Phys. Lett. 49, 998 (1986).

Gary M. Carter, "Excited-state dynamics and temporally resolved nonresonant nonlinear-optical processes in polydiacetylenes," J. Opt. Soc. Am. B 4, 1018 (1987).

M.K. Casstevens, M. Samoc, J. Pfleger, and P.N. Prasad, "Dynamics of third-order nonlinear optical processes in Langmuir-Blodgett and evaporated films of phthalocyanines," J. Chem. Phys. 92, 2019 (1990).

D.S. Chemla and J. Zyss, eds., *Nonlinear Optical Properties of Organic and Polymeric Materials* (Academic Press, Orlando, 1987).

A.J. Dann, H. Hoshi, Y. Maruyama, "The structure and properties of phthalocyanine films grown by the molecular beam epitaxy technique. I. Preparation and characterization," J. Appl. Phys. 67, 1371 (1990).

M.F. Dautartas, S.Y. Suh, S.R. Forrest, and M.L. Kaplan, "Optical recording using hydrogen phthalocyanine thin films, " Appl. Phys. A, 36, 71 (1985).

J.-C.M. Diels, J.J. Fontaine, I.C. McMichael, and F. Simoni, "Control and measurement of ultrashort pulse shapes (in amplitude and phase) with femtosecond accuracy," Appl. Opt. 24, 1270 (1985).

W. Dietel, "Transient absorber gratings shorten the pulses of a passively mode-locked cw dye laser," Opt. Comm. 43, 69 (1982).

W. Dietel, E. Döpel, D. Kühlke, and B. Wilhelmi, "Pulses in the femtosecond range from a cw dye ring laser in the colliding pulse mode-locking (CPM) regime with down-chirp," Opt. Comm. 43, 433 (1982).

W. Dietel, J.J. Fontaine, and J.-C. Diels, "Intracavity pulse compression with glass: A new method of generating pulses shorter than 60 fsec," Opt. Lett. 8, 4 (1983).

S.N. Dixit, D. Guo, and S. Mazumdar, "Essential-states mechanism of optical nonlinearity in π-conjugated polymers," Phys. Rev. B 43, 6781 (1991).

D. Djurado, C. Fabre, A. Hamwi, and J.C. Cousseins, "High resolution solid-state ^{13}C CPMAS study of neutral and partially oxidized aluminum polyfluorophthalocyanines," Synth. Met. 22, 121 (1987).

B. Fluegel, N. Peyghambarian, G. Olbright, M. Lindberg, S.W. Koch, M. Joffre, D. Hulin, A. Migus, and A. Antonetti, "Femtosecond studies of coherent transients in semiconductors," Phys. Rev. Lett. 59, 2588 (1987).

R.L. Fork, B.I. Greene, and C.V. Shank, "Generation of optical pulses shorter than 0.1 psec by colliding pulse mode locking," Appl. Phys. Lett. 38, 671 (1981).

R.L. Fork, C.V. Shank, and R.T. Yen, "Amplification of 70-fs optical pulses to gigawatt powers," Appl. Phys. Lett. 41, 223 (1982).

R.L. Fork, C.V. Shank, C. Hirlimann, R. Yen, and W.J. Tomlinson, "Femtosecond white-light continuum pulses," Opt. Lett. 8, 1 (1983).

R.L. Fork, O.E. Martinez, and J.P. Gordon, "Negative dispersion using pairs of prisms," Opt. Lett. 9, 150 (1984).

R.L. Fork, C.H. Brito-Cruz, P.C. Becker, and C.V. Shank, "Compression of optical pulses to six femtoseconds by using cubic phase compensation," Opt. Lett. 12, 483 (1987).

A.F. Garito and J.W. Wu, "Optical bistability in random glassy polymers," SPIE 1147, 2 (1989).

H.M. Gibbs, G. Khitrova, and N. Peyghambarian eds., *Nonlinear Photonics* (Springer Verlag, Berlin, 1990).

A.S.L. Gomes, A.S. Gouveia-Neto, and J.R. Taylor, "Optical fibre-grating pulse compressors," Opt. and Quant. Electron. 20, 95 (1988).

Y. Goto, N. Koshino, K. Itoh, "Tellurium and copper-phthalocyanine multilayer films for optical disk media," Jufitsu Sci. Tech. J. 20, 411 (1984).

B.I. Greene and R.R. Millard, "Singlet-exciton fusion in molecular solids: A direct subpicosecond determination of time-dependent annihilation rates," Phys. Rev. Lett. 55, 1331 (1985a).

B.I. Greene and R.R. Millard, "Subpicosecond spectroscopic studies of singlet fusion in molecular solids," J. de Physique, Colloque C7, C7-371 (1985b).

B.I. Greene, J. Orenstein, R.R. Millard, and L.R. Williams, "Picosecond relaxation dynamics in polydiacetylene-*pts*," Chem. Phys. Lett. 139, 381 (1987).

H.A. Haus, "Theory of mode locking with a slow saturable absorber," IEEE J. Quant. Electron. QE-11, 736 (1975).

H.A. Haus, C.V. Shank, and E.P. Ippen, "Shape of passively mode-locked laser pulses," Opt. Comm. 15, 29 (1975).

J.R. Heflin, K.Y. Wong, O. Zamani-Khamiri, and A.F. Garito, "Nonlinear optical properties of linear chains and electron-correlation effects," Phys. Rev. B 38, 1573 (1988).

T.F. Heinz, S.L. Palfrey, and K.B. Eisenthal, "Coherent coupling effects in pump-probe measurements with collinear, copropagating beams," Opt. Lett. 9, 359 (1984).

P.P. Ho, R. Dorsinville, N.L. Yang, G. Odian, G. Eichmann, T. Jimbo, Q.Z. Wang, G.C. Tang, N.D. Chen, W.K. Zou, Y. Li, and R.R. Alfano, "Ultrafast nonlinear optical processes in 4BCMU-polydiacetylene," SPIE 682, 36 (1986).

Z.Z. Ho, C.Y. Ju, and W.M. Hetherington III, "Third harmonic generation in phthalocyanines," J. Appl. Phys. 62, 716 (1987).

Z.Z. Ho and N. Peyghambarian, "Femtosecond dynamics in organic thin films of fluoro-aluminum phthalocyanine," Chem. Phys. Lett. 148, 107 (1988).

H. Hoshi, A.J. Dann, and Y. Maruyama, "The structure and properties of phthalocyanine films grown by the molecular-beam epitaxy technique. II. Ultraviolet/visible spectroscopic study," J. Appl. Phys. 67, 1845 (1990).

T. Huang, K.E. Rieckhoff, E. Voight, and E.R. Menzel, "Spin-orbit effects in metalphthalocyanines," Chem. Phys. 19, 25 (1977).

D. Hulin, A. Mysyrowicz, A. Antonetti, A. Migus, W.T. Masselink, H. Morkoç, H.M. Gibbs, and N. Peyghambarian, "Ultrafast all-optical gate with subpicosecond ON and OFF response time," Appl. Phys. Lett. 49, 749 (1986).

E.P. Ippen, C.V. Shank, and A. Dienes, "Passive mode locking of the cw dye laser," Appl. Phys. Lett. 21, 348 (1972).

E.P. Ippen and C.V. Shank, "Dynamic spectroscopy and subpicosecond pulse compression," Appl. Phys. Lett. 27, 488 (1975).

C. Jennings, R. Aroca, A.-M. Hor, and R.O. Loutfy, "Raman spectra of solid films - V. Chloroaluminum, chlorogallium and chloroindium phthalocyanine complexes," Spectrochimica Acta 42A, 991 (1986).

J.L. Jewell, Y.H. Lee, M. Warren, H.M. Gibbs, N. Peyghambarian, A.C. Gossard, and W. Wiegmann, "3-pJ, 82-MHz optical logic gates in a room-temperature GaAs-AlGaAs multiple-quantum-well étalon," Appl. Phys. Lett. 46, 918 (1985).

R. Jin. J.P. Sokoloff, P.A. Harten, C.L. Chuang, S.G. Lee, M. Warren, H.M. Gibbs, N. Peyghambarian, J.N. Polky, and G.A. Pubanz, "Ultrafast modulation with subpicosecond recovery time in a GaAs/AlGaAs nonlinear directional coupler," Appl. Phys. Lett. **56**, 993 (1990).

M. Joffre, D. Hulin, A. Migus, A. Antonetti, C. Benoit à la Guillaume, N. Peyghambarian, M. Lindberg, and S.W. Koch, "Coherent effects in pump-probe spectroscopy of excitons," Opt. Lett. **13**, 276 (1988).

F. Kajzar, S. Etemad, G.L. Baker, and J. Messier, "Frequency dependence of the large, electronic $\chi^{(3)}$ in polyacetylene," Solid State Commun. **63**, 1113 (1987).

F. Kajzar, L. Rothberg, S. Etemad, P.A. Chollet, D. Grec, A. Boudet, and T. Jedju, "Saturation absorption and Kerr susceptibility in polydiacetylene langmuir-blodgett film," Opt. Comm. **66**, 55 (1988).

A. Kalbeitzal, D. Neher, C. Bubeck, T. Sauer, G. Wegner, and W. Caseri, "Influence of the film preparation on the nonlinear optical properties of phthalocyanine films," in *Electronic Properties of Conjugated Polymers III*, ed. by H. Kuzmany, M. Mehring and S. Roth, Springer Series in Solid State Sciences, Vol. 91 (Springer-Verlag, Berlin, (1989).

M. Kasha, "Molecular excitons in small aggregates," in *Spectroscopy of the Excited State*, edited by B. DiBartolo (Plenum Press, New York, 1976) p. 337.

G.A. Kenney-Wallace, "Picosecond laser spectroscopy and molecular dynamics: I Pump-probe spectroscopy techniques and photodynamics II Nonlinear laser spectroscopy and molecular motion," and reference therein in *Molecular Liquids. Dynamics and Interactions*, ed. by A.J. Barnes, W.J. Orville-Thomas, and J. Yarwood, NATO ASI Series, Series C: Mathematical and Physical Sciences, Vol. 135 (D. Reidel Publishing Co., Dordrecht, 1984) pp. 331-356.

E.V. Khoroshilov, I.V. Kryukov, P.G. Kryukov, and A.V. Sharkov, "10 kHz-rate amplification of 40-fs optical pulses at low pumping energy," in *Ultrafast Phenomena VI*, ed. by T. Yajima, K. Yoshihara, C.B. Harris, and S. Shionoya. (Springer-Verlag, Berlin, 1988) p. 22.

T.J. Klofta, P.C. Rieke, C.A. Linkous, W.J. Buttner, A. Nanthakumar, T.D. Mewborn, and N.R. Armstrong, "Tri- and tetravalent phthalocyanine thin film photoelectrodes: Comparison with other metal and demetallated phthalocyanine systems," J. Electrochem. Soc. **132**, 2134 (1985) and references therein.

W.H. Knox, M.C. Downer, R.L. Fork, and C.V. Shank, "Amplified femtosecond optical pulses and continuum generation a 5-kHz repetition rate," Opt. Lett. **9**, 552 (1984).

W.H. Knox, C. Hirlimann, D.A.B. Miller, J. Shah, D.S. Chemla, and C.V. Shank, "Femtosecond excitation of nonthermal carrier populations in GaAs quantum wells," Phys. Rev. Lett. **56**, 1191 (1986).

W.H. Knox, "Femtosecond optical pulse amplification," IEEE J. Quant. Electron. 24, 388 (1988).

W.H. Knox, D.S. Chemla, G. Livescu, J.E. Cunningham, and J.E. Henry, "Femtosecond carrier thermalization in dense fermi seas," Phys. Rev. Lett. 61, 1290 (1988).

M. Kobayashi, A. Yabe, Y. Maeno, K. Oishi, K. Kawamura, and S. Ohno, "Erasable optical memory with thermoplastic/absorbent double layer," Appl. Phys. Lett., 52, 1777 (1988).

T. Kobayashi and S. Nagakura, "Bimolecular quenching of fluorescence and interaction between excited molecules in solution," Molec. Phys. 23, 1211 (1972a).

T. Kobayashi and S. Nagakura, "The biexcitonic quenching and exciton migration rate in aromatic crystals," Mol. Phys. 24, 695 (1972b).

W.F. Kosonocky, S.E. Harrison, and R. Stander, "Observations of the triplet state in phthalocyanines," J. Chem. Phys. 43, 831 (1965).

H. Laurs and G. Heiland "Electrical and optical properties of phthalocyanine films," Thin Solid Films 149, 129 (1987).

W.-Z. Lin, R.W. Schoenlein, J.G. Fujimoto, and E.P. Ippen, "Femtosecond absorption saturation studies of hot carriers in GaAs and AlGaAs," IEEE J. Quant. Electron. 24, 267 (1988).

M. Lindberg and S.W. Koch, "Theory of coherent transients in semiconductor pump-probe spectroscopy," J. Opt. Soc. Am. B 5, 139 (1988a).

M. Lindberg and S.W. Koch, "Transient oscillations and dynamic Stark effect in semiconductors," Phys. Rev. B 38, 7606 (1988b).

J.P. Linsky, T.R. Paul, R.S. Nohr, and M.E. Kenney, "Studies of a series of haloaluminum, -gallium, and -indium phthalocyanines," Inorg. Chem. 19, 3131 (1980).

R.F. Loring, Y.J. Yan, and S. Mukamel, "Hole-burning spectroscopy of polar molecules in polar solvents: Solvation dynamics and vibrational relaxation," J. Phys. Chem. 91, 1302 (1987).

D. Markovitsi and I. Lécuyer, "Laser-induced triplet excitons in the columnar phases of an octasubstituted zinc phthalocyanine," Chem. Phys. Lett. 149, 330 (1988).

D. Markovitsi, T.-H. Tran-Thi, V. Briois, J. Simon, and K. Ohta, "Laser induced triplet excitons in the columnar phases of an octasubstituted metal free phthalocyanine," J. Am. Chem. Soc. 110, 2001 (1988).

T.J. Marks, "Electrically conductive metallomacrocyclic assemblies," Science (Washington D.C.) 227, 881 (1985).

O.E. Martinez, R.L. Fork, and J.P. Gordon, "Theory of passively mode-locked lasers including self-phase modulation and group-velocity dispersion," Opt. Lett. 9, 156 (1984).

R.A. Mathies, W.T. Pollard, C.H. Brito Cruz, and C.V. Shank, "Direct observation of the femtosecond excited-state cis-trans isomerization in bacteriorhodopsin," in *Ultrafast Phenomena VI*, ed. by T. Yajima, K. Yoshihara, C.B. Harris, and S. Shionoya (Springer-Verlag, Berlin, 1988a) p. 584.

R.A. Mathies, C.H. Brito Cruz, W.T. Pollard, C.V. Shank, "Direct observation of the femtosecond excited-state *cis-trans* isomerization in bacteriorhodopsin," Science 240, 777 (1988b).

J. McVie, R.S. Sinclair, and T.G. Truscott, "Triplet states of copper and metal-free phthalocyanines, J. Chem. Soc. Faraday Trans. II 74, 1870 (1978).

E.R. Menzel, K.E. Rieckhoff, and E.M. Voigt, "Relaxation mechanisms from excited singlet states and the effect of spin-orbit coupling," Chem. Phys. Lett. 13, 604 (1972).

E.R. Menzel and J.H. Sharp, "Singlet-triplet fusion in metal-free phthalocyanine," J. Chem. Phys. 66, 67 (1977).

A. Migus, A. Antonetti, J. Etchepare, D. Hulin, and A. Orszag, "Femtosecond spectroscopy with high-power tunable optical pulses," J. Opt. Soc. Am. B 2, 584 (1985).

R.R. Millard and B.I. Greene, "Direct determination of nonradiative relaxation rates in nonfluorescent metallophthalocyanines," J. Chem Phys. 89, 2976 (1985).

R.R. Millard and B.I. Greene, "Singlet exciton fusion in molecular solids," Springer Ser. Chem. Phys. 46 (Ultrafast Phenom. 5), 478 (1986).

K.W. Nebesny, G.E. Collins, P.A. Lee, L.-K. Chau, J. Danziger, E. Osburn, and N.R. Armstrong, "Organic/inorganic - molecular beam epitaxy (O/I-MBE): Formation of an ordered phthalocyanine/SnS_2 heterojunction," submitted to Chem. of Matr. (1991).

D. Neher, A. Kaltbeitzel, A. Wolf, C. Bubeck, and G. Wegner, "Nonlinear optical properties of ultrathin polymer films," in *Conjugated Polymeric Materials: Opportunities in Electronics, Opto-Electronics and Molecular Electronics*, ed. by J.L. Brédas and R.R. Chance, NATO ASI Series (Kluwer Acad. Publ., Dordrecht, 1990) pp. 387-398.

W.L. Nighan Jr., private communication (1991).

G. R. Olbright, "Femtosecond dynamics and nonlinear effects of electron-hole plasma in semiconductor doped glasses," Ph.D. Dissertation (University of Arizona, 1987) p. 41.

J.L. Oudar and D.S. Chemla, "Theory of second-order susceptibilities of benzene substitutes," Opt. Comm. 13, 164 (1975).

J.L. Oudar, D. Hulin, A. Migus, A. Antonetti, and F. Alexandre, "Subpicosecond spectral hole burning due to nonthermalized photoexcited carriers in GaAs," Phys. Rev. Lett. **55**, 2074 (1985).

S.L. Palfrey and T.F. Heinz, "Coherent interactions in pump-probe absorption measurements: The effect of phase gratings," J. Opt. Soc. Am. B **2**, 674 (1985).

W.T. Pollard, C.H. Brito Cruz, C.V. Shank, R.A. Mathies, "Direct observation of the excited-state *cis-trans* photoisomerization of bacteriorhodopsin: Multilevel line shape theory for femtosecond dynamic hole burning and its application," J. Chem. Phys. **90**, 199 (1989).

R.C. Powell and Z.G. Soos, "Review Article. Singlet exciton energy transfer in organic solids," J. Luminescence **11**, 1 (1975).

P.N. Prasad, "Nonlinear optical effects in organic molecules and polymers - theory, measurements, and devices," SPIE **1017**, 2 (1988a).

P.N. Prasad, "Third order nonlinear optical effects in organic polymeric films," Mat. Res. Soc. Symp. Proc. **109** (Nonlinear Opt. Prop. Poly.), 271 (1988b).

P.C. Rieke, "Photoelectrochemistry of thin film chloro-gallium phthalocyanine electrodes for solar energy conversion," Ph.D. dissertation (University of Arizona, 1984).

G.W. Robinson and R.P. Frosch, "Electronic excitation transfer and relaxation," J. Chem. Phys. **38**, 1187 (1983).

I.S. Ruddock and D.J. Bradley, "Bandwidth-limited subpicosecond pulse generation in mode-locked cw dye lasers," Appl. Phys. Lett. **29**, 296 (1976).

T. Sauer, W. Caser, and G. Wegner, "Novel phthalocyanine polymers for applications in optical devices," Mol. Cryst. Liq. Cryst. **183**, 387 (1990).

C. Sauteret, J.-P. Hermann, R. Frey, F. Pradère, J. Ducuing, R.H. Baughman, and R.R. Chance, "Optical nonlinearities in one-dimensional-conjugated polymer crystals," Phys. Rev. Lett. **36**, 956 (1976).

B. Sermage, J.P. Heritage, and N.K. Dutta, "Temperature dependence of carrier lifetime and Auger recombination in 1.3μm InGaAsP," J. Appl. Phys. **57**, 5443 (1985).

C.V. Shank and E.P. Ippen, "Subpicosecond kilowatt pulses from a mode-locked cw dye laser," Appl. Phys. Lett. **24**, 373 (1974).

C.V. Shank, R.L. Fork, R. Yen, R.H. Stolen, and W.J. Tomlinson, "Compression of femtosecond optical pulses," Appl. Phys. Lett. **40**, 761 (1982).

C.V. Shank, R.L. Fork, C.H. Brito Cruz, and W. Knox, "Investigations of nonthermal population distributions with 10-fs optical pulses," in *Ultrafast Phenomena V*, ed. by G.R. Fleming and A.E. Siegman (Springer-Verlag, Berlin, 1986).

Y.R. Shen, *The Principles of Nonlinear Optics* (Wiley and Sons, New York, 1984).

Anthony E. Siegman, *Lasers* (University Science Books, Mill Valley, 1986) pp. 1057-1058, 1104-1128.

J. Simon and J.-J. André, "Ch. III Metallophthalocyanines," in *Molecular Semiconductors*, ed. by J.M. Lehn and Ch. W. Rees (Springer-Verlag, Berlin, 1985) pp. 73-149.

T.D. Sims, J.E. Pemberton, P.A. Lee, and N.R. Armstrong, "Comparison of supramolecular aggregate structure and spectroscopic and photoelectrochemical properties of tetravalent and trivalent metal phthalocyanine thin films," Chemistry Matr. 1, 26 (1989).

J.P. Sokoloff, M. Joffre, B. Fluegel, D. Hulin, M. Lindberg, S.W. Koch, A. Migus, A. Antonetti, and N. Peyghambarian, "Transient oscillations in the vicinity of excitons and in the band of semiconductors," Phys. Rev. B 38, 7615 (1988).

G.I. Stegeman, R. Zanoni, and C.T. Seaton, "Nonlinear organic materials in integrated optics structures," Mat. Res. Symp. Proc. 109, 53 (1989).

A. Suna, "Kinematics of exciton-exciton annihilation in molecular crystals," Phys. Rev. B 1, 1716 (1970).

P.D. Townsend, J.L. Jackel, G.L. Baker, J.A. Shelburne, III, and S. Etemad, "Observation of nonlinear optical transmission and switching phenomena in polydiacetylene-based directional couplers," Appl. Phys. Lett. 55, 1829 (1989).

E.B. Treacy, "Optical pulse compression with diffraction gratings," IEEE J. Quant. Electron. QE-5, 454 (1969).

T.J. Trout, S. Velsko, R. Bozio, P.L. Decola, and R.M. Hochstrasser, "Nonlinear raman study of line shapes and relaxation of vibrational states of isotropically pure and mixed crystals of benzene," J. Chem. Phys. 81, 4746 (1984).

J.A. Valdmanis, R.L. Fork, and J.P. Gordon, "Generation of optical pulses as short as 27 femtoseconds directly from a laser balancing self-phase modulation, group-velocity dispersion, saturable absorption, and saturable gain," Opt. Lett. 10, 131 (1985).

P.S. Vincett, E.M. Voigt, and K.E. Rieckhoff, "Phosphorescence and fluorescence of phthalocyanines," J. Chem. Phys. 55, 4131 (1970).

W. Vogel, D.-G. Welsch, and B. Wilhelmi, "Time-resolved spectral hole burning," Chem. Phys. Lett. 153, 376 (1988).

V.S. Williams, G.R. Olbright, B.D. Fluegel, S.W. Koch, and N. Peyghambarian, "Optical nonlinearities and ultrafast carrier dynamics in semiconductor doped glasses," J. Mod. Optics 35, 1979 (1988).

V.S. Williams, Z.Z. Ho, N. Peyghambarian, W.M. Gibbons, R.P. Grasso, M.K. O'Brien, P.J. Shannon, and S.T. Sun, "Picosecond all-optical logic gate in a nonlinear organic étalon," Appl. Phys. Lett. 57, 2399 (1990).

V.S. Williams, J.P. Sokoloff, Z.Z. Ho, C. Arbour, N.R. Armstrong, and N. Peyghambarian, "Observation of polarization-dependent spectral holes in an organic thin film," QELS (1991a).

V.S. Williams, J.P. Sokoloff, Z.Z. Ho, C. Arbour, N.R. Armstrong, and N. Peyghambarian, "Polarization-dependent spectral hole-burning in a fluoro-aluminum phthalocyanine organic thin film," submitted to Chem. Phys. Lett. (1991b).

K. Yoshino, K. Kaneto, and Y. Inuishi, "Photoconduction and emission of phthalocyanine in the near infrared," in *Energy and Charge Transfer in Organic Semiconductors*, ed. by K. Masuda and M. Silver (Plenum Press, New York, 1974).

M.T. Zhao, B.P. Singh, and P.N. Prasad, "A systematic study of polarizability and microscopic third-order optical nonlinearity in thiophene oligomers," J. Chem. Phys. 89, 5535 (1988).

M.T. Zhao, M. Samoc, B.P. Singh, and P.N. Prasad, "Study of third order microscopic optical nonlinearities in sequentially built and systematically derivatized structures," J. Phys. Chem. 93, 7916 (1989).

Z.F. Zhu and E. Garmire, "Optical bistability in four-level nonradiative dyes," Opt. Comm. 46, 61 (1983).